ESAIM: M2AN 58 (2024) 2079–2115
https://doi.org/10.1051/m2an/2024070

ESAIM: Mathematical Modelling and Numerical Analysis
www.esaim-m2an.org

NITSCHE METHOD FOR NAVIER–STOKES EQUATIONS WITH SLIP BOUNDARY CONDITIONS: CONVERGENCE ANALYSIS AND VMS-LES STABILIZATION

Aparna Bansal[1], Nicolás A. Barnafi[2,3] and Dwijendra Narain Pandey[1,*]

Abstract. In this paper, we analyze Nitsche's method for the stationary Navier–Stokes equations on Lipschitz domains under minimal regularity assumptions. Our analysis provides a robust formulation for implementing slip (*i.e.*, Navier) boundary conditions in arbitrarily complex boundaries. The well-posedness of the discrete problem is established using the Banach Nečas–Babuška and Banach fixed point theorems under standard small data assumptions. We also provide optimal convergence rates for the approximation error. Furthermore, we propose a quasi-static VMS-LES formulation with Nitsche for the Navier–Stokes equations with slip boundary conditions to address the simulation of incompressible fluids at high Reynolds numbers. We validate our theory through several numerical tests in well-established benchmark problems.

Mathematics Subject Classification. 65N30, 65N12, 65N15, 65J15, 76D07.

Received August 12, 2023. Accepted September 5, 2024.

1. Introduction

The Navier–Stokes equations describe the motion of incompressible fluids and pose significant challenges across different disciplines. The numerical analysis community has put considerable effort into developing robust and efficient techniques for their numerical approximation. It is typically assumed that the fluid adheres to its recipient's walls, known as the no-slip boundary condition. The accuracy of this assumption has been a subject of intense debate [33]. There are several scenarios where slip boundary conditions are more appropriate, such as inkjet printing [45], pipe flow [10], complex turbulent flows [28], and slide coating [17]. These situations require the consideration of slip/Navier boundary conditions for accurate description. Slip boundary conditions are crucial in microfluidics and nanofluidics, where fluid flow occurs at small scales. This is a well understood phenomenon in statistical mechanics, where the Navier–Stokes equations have been shown to solve the Boltzmann for small Knudsen number [56]. This field is known as generalized slip-flow theory.

Keywords and phrases. Navier–Stokes equations, Navier boundary conditions, Nitsche's method, Banach fixed point theorem, Banach–Nečas–Babuška theorem, *a priori* analysis, variational multiscale modeling, large eddy simulation.

[1] Department of Mathematics, Indian Institute of Technology Roorkee, Roorkee 247667, India.

[2] Instituto de Ingeniería Matemática y Computacional & Facultad de Ciencias Biológicas, Pontificia Universidad Católica de Chile, Av. Vicuña Mackenna, 4860 Santiago, Chile.

[3] Centro de Modelamiento Matemático (CNRS IRL2807), Santiago, Chile.

[*]Corresponding author: dwijpfma@iitr.ac.in

Navier boundary conditions impose a constraint only in the normal direction of the flow velocity, which can make the implementation not trivial. The first method to enforce slip conditions weakly was through a Lagrange multiplier; see [44, 61, 62]. However, the Lagrange multiplier method introduces additional computational costs due to the addition of an extra degree of freedom in the discrete domain. Further studies have been devoted to penalty methods that enforce the slip conditions using a regularization term; see [4, 6, 55]. This method is inconsistent and requires additional regularity from the solution, but they remain popular due to their simplicity. For the Navier–Stokes/Stokes equations with slip conditions, works with Lagrange multiplier and penalty methods were also developed [13, 23, 24, 60], with emphasis on the case of curved boundaries, where a Babuška type paradox may appear. Other recent studies have focused on using penalty terms along with Lagrange finite elements [41, 67, 68] and Crouzeix–Raviart finite elements [42, 69], which adequately characterize the impact of the variational crimes.

The Nitsche method was proposed by Nitsche [48] and is a consistent boundary penalty technique to incorporate Dirichlet boundary conditions. Several variants of the Nitsche method exist, but our work is grounded in the symmetric variant. Numerous references present the symmetric variant of the Nitsche method; refer to [16, 35, 57, 59]. In this formulation, it is necessary for the value of the stabilization parameter γ to be sufficiently large to guarantee well-posedness, but not excessively large, as the slip error diminishes with arbitrarily large values of γ. A specific treatment of the Navier boundary condition has been examined in [66], based on the Nitsche method developed by Juntunen and Stenberg [40] to discretize robustly Robin-type boundary conditions. Gjerde and Scott [31] provide the best convergence rate that can be expected for a polygonal approximation of a curved boundary by considering the projection of the normal and tangent vectors, thus avoiding the paradox. Finally, we highlight that Araya *et al.* [2] discussed both symmetric and non-symmetric variants of Nitsche for imposing slip boundary conditions on the Stokes equations with stabilized finite elements.

The turbulent behavior of the Navier–Stokes equations for high Reynolds numbers gives rise to numerical instabilities that make their numerical approximation very challenging and severely impact the accuracy of the finite element method. The most common strategies for modeling turbulent flows are direct numerical simulations (DNS), Reynolds averaged Navier–Stokes equations (RANS), and large eddy simulations (LES). LES methods are more accurate than RANS [34] and less computationally intensive than DNS [47, 53]. DNS simulations achieve complete resolution of features without employing models, but their major limitation lies in their high computational cost, rendering them impractical for most cases. Conversely, with LES, only the large scale features of the flow field are fully represented. Unresolved scales are managed using models based on the resolved scales, thus making the computational costs more affordable. The weak imposition of the no-slip boundary conditions for turbulent flows is discussed in [8]. The first attempts to perform LES using the Variational Multiscale (VMS) framework as presented in [37–39, 43], involved the introduction of an explicit LES model to account for the stress tensor at small scales. The VMS-LES scheme uses projectional methods, splitting the continuous unknown into a resolvable FE (finite element) component and an unresolvable subscale component. The action of the unresolvable component onto the FE scales is approximated in various ways, resulting in different VMS models based on residual, ensuring consistency. The formulation of adequate subscale models has been an intense research topic, see [18–20] for subgrid scale modeling, and [9, 22, 27, 50] for VMS based models.

Our main contribution is twofold: on the one hand, we provide a complete convergence analysis of the slip boundary condition for the stationary Navier–Stokes equations on a polygonal boundary using a symmetric variant of Nitsche's method. On the other hand, we propose a quasi-static VMS-LES formulation with Nitsche to address behavior of an incompressible flows at high Reynolds number with slip boundary conditions. Finally, numerical examples are provided to verify the theoretical findings and to test our stabilized formulation on benchmark problems with high Reynolds numbers.

1.1. Outline of the paper

In Section 2, we present the Navier–Stokes equations with the slip boundary condition, derive the weak formulation of the problem, and then discuss the solvability analysis of the continuous case. In Section 3, we introduce the Nitsche scheme, then derive the variational formulation and establish the well-posedness of the discrete Oseen problem using the Banach Nečas Babuška theorem. The well-posedness result is extended to the Navier–Stokes equations using Banach's fixed point theorem in a standard way. In Section 4, we derive *a priori* estimate and prove the optimal convergence of the method. In Section 5, we propose a quasi-static VMS-LES formulation with Nitsche for the Navier–Stokes equations with slip boundary conditions to address behavior of flows at high Reynolds numbers. Therefore, we consider the unsteady case to overcome the challenges associated with the stationary Navier–Stokes equations when studying numerical simulations at high Reynolds numbers. In Section 6, we perform some numerical tests to support our theoretical results. The first one validates the theoretical results of the Nitsche scheme and collects computational results consisting of verification of spatio-temporal convergence for high Reynolds numbers. Finally, computational tests on benchmark problems, one on the lid-driven cavity problem and the other on flow past through a circular cylinder with high Reynolds numbers, are discussed. We also compare the results with slip and no-slip boundary conditions.

1.2. Notations and preliminaries

Let $\Omega \subseteq \mathbb{R}^d, d \in \{2,3\}$ be an open and bounded domain with a Lipschitz polygonal boundary Γ. The Sobolev spaces are denoted by $W^{s,p}(\Omega)$ with $s \geq 0$. They contain all $L^p(\Omega)$ with $p \geq 1$ functions whose distributional derivative up to order s are in $L^p(\Omega)$. The norm and seminorm in $W^{s,p}(\Omega)$ are denoted by $\|\cdot\|_{s,p,\Omega}$ and $|\cdot|_{s,p,\Omega}$. For $p=2$, $W^{s,p}(\Omega)$ is denoted by $H^s(\Omega)$ and its corresponding norm and seminorm is denoted by $\|\cdot\|_{s,\Omega} := \|\cdot\|_{s,2,\Omega}$ and $|\cdot|_{s,\Omega} :=|\cdot|_{s,2,\Omega}$, respectively. The space $L^2_0(\Omega)$ represents all L^2 functions with average zero condition over Ω. The vector-valued Sobolev spaces will be represented using boldface letters as $\boldsymbol{H}^s(\Omega)$. Additionally, we will denote with $H^1_{\Gamma_a}(\Omega)$ the subspace of $H^1(\Omega)$ with homogeneous boundary conditions on Γ_a (or $H^1_0(\Omega)$ when $\Gamma_a = \Gamma$), for which the Friedrichs-Poincarè inequality holds [21] *i.e.*, there exists $C_{\mathrm{FP}} > 0$ which depends on Ω and Γ_a such that

$$\|f\|_{1,\Omega} \leq C_{\mathrm{FP}} |f|_{1,\Omega} \quad \forall f \in H^1_{\Gamma_a}(\Omega). \tag{1}$$

The Hölder inequality is given by

$$\int_\Omega |fg| \leq \|f\|_{L^p(\Omega)} \|g\|_{L^q(\Omega)}, \quad \forall f \in L^p(\Omega),\ \forall g \in L^q(\Omega), \quad \text{with} \quad \frac{1}{p} + \frac{1}{q} = 1. \tag{2}$$

We have that the following Sobolev embedding $H^1(\Omega) \hookrightarrow L^q(\Omega)$ holds for $1 \leq q < \infty$ when $d=2$ and $1 \leq q \leq 6$ when $d=3$. In particular, there exists a constant $C_{\mathrm{Sob}}\,(q,d) > 0$, that depends only on the domain, such that

$$\|f\|_{0,q,\Omega} \leq C_{\mathrm{Sob}}(q,n) \|g\|_{1,\Omega} \ \ \text{for} \begin{cases} q \geq 1 & \text{if } d=2, \\ q \in [1,6] & \text{if } d=3. \end{cases} \tag{3}$$

Finally, we will consider the norm of a product space $\mathrm{V} \times \Pi$ to be $\|(\cdot,\cdot)\| = \|\cdot\|_{\mathrm{V}} + \|\cdot\|_{\Pi}$. Also, whenever an inequality holds for positive constants that do not depend on the mesh size, we write $\lesssim$ or $\gtrsim$ and omit the constants.

2. Continuous problem

In this section, we introduce the model problem, define the weak formulation, discuss the stability properties, and finally prove the existence and uniqueness of the solution.

2.1. The model problem

The stationary incompressible Navier–Stokes equations are stated as follows

$$\begin{aligned} -\nu\Delta\boldsymbol{u} + (\boldsymbol{u}\cdot\nabla)\boldsymbol{u} + \nabla p = \boldsymbol{f} \quad & \text{in}\,\Omega, \\ \operatorname{div}\boldsymbol{u} = 0 \quad & \text{in}\,\Omega, \\ \boldsymbol{u} = \boldsymbol{0} \quad & \text{on}\,\Gamma_D, \\ \int_\Omega p\,\mathrm{d}x = 0, & \end{aligned} \tag{4}$$

posed on a spatial domain $\Omega \subseteq \mathbb{R}^d, d \in \{2,3\}$ with Lipschitz boundary Γ, where $\boldsymbol{u}$ is the fluid velocity, $\nu > 0$ is the viscosity, p is the fluid pressure and $\boldsymbol{f}$ represents the external body force on Ω. The Navier boundary condition on Γ_{Nav} is defined as

$$\begin{aligned} \boldsymbol{u}\cdot\boldsymbol{n} = 0 \quad & \text{on}\,\Gamma_{\mathrm{Nav}}, \\ \nu\boldsymbol{n}^t D(\boldsymbol{u})\boldsymbol{\tau}^i + \beta\boldsymbol{u}\cdot\boldsymbol{\tau}^i = 0 \quad & \text{on}\,\Gamma_{\mathrm{Nav}}, \quad i = 1,\dots(d-1) \end{aligned} \tag{5}$$

where the boundary $\Gamma = \overline{\Gamma}_D \cup \overline{\Gamma}_{\mathrm{Nav}}$ and $\Gamma_D \cap \Gamma_{\mathrm{Nav}} = \emptyset$. The Navier boundary condition allows the fluid to slip along the boundary. It requires that the tangential component of the stress vector at the boundary be proportional to the tangential velocity. The strain tensor is denoted by $D(\boldsymbol{u}) = \nabla\boldsymbol{u} + (\nabla\boldsymbol{u})^T$, and $\boldsymbol{n}$ and $\boldsymbol{\tau}^i$ are unit normal and tangent vectors to the boundary Γ. The friction coefficient β will require some controlled behavior for well-posedness, as shown in Lemma 3. The assumption of homogeneity in the boundary conditions is made to simplify the subsequent analysis, as lifting operators have already been established [42]. Non-homogeneous boundary conditions are utilized in the numerical tests in Section 6.

2.2. Weak formulation of the continuous problem

Define the spaces:

$$\begin{aligned} \mathrm{V} &\coloneqq \left\{\boldsymbol{v} \in \boldsymbol{H}^1(\Omega) :\, \boldsymbol{v}\cdot\boldsymbol{n} = 0 \text{ on } \Gamma_{\mathrm{Nav}}, \boldsymbol{v} = \boldsymbol{0} \text{ on } \Gamma_D\right\}, \\ \Pi &\coloneqq L^2_0(\Omega). \end{aligned}$$

The standard weak formulation of (4) and (5) is given by: Find $(\boldsymbol{u}, p) \in \mathrm{V}\times\Pi$, such that

$$\mathcal{A}[(\boldsymbol{u}, p); (\boldsymbol{v}, q)] = \mathcal{F}(\boldsymbol{v}) \quad \forall(\boldsymbol{v}, q) \in \mathrm{V}\times\Pi, \tag{6}$$

where

$$\begin{aligned} \mathcal{A}[(\boldsymbol{u}, p); (\boldsymbol{v}, q)] \coloneqq{}& \frac{\nu}{2}(D(\boldsymbol{u}), D(\boldsymbol{v}))_\Omega + (\boldsymbol{u}\cdot\nabla\boldsymbol{u}, \boldsymbol{v})_\Omega - (p, \nabla\cdot\boldsymbol{v})_\Omega - (q, \nabla\cdot\boldsymbol{u})_\Omega \\ &+ \int_{\Gamma_{\mathrm{Nav}}} \beta\sum_i^{d-1}\left(\boldsymbol{\tau}^i\cdot\boldsymbol{v}\right)\left(\boldsymbol{\tau}^i\cdot\boldsymbol{u}\right)\mathrm{d}s, \\ \mathcal{F}(\boldsymbol{v}) \coloneqq{}& \langle\boldsymbol{f}, \boldsymbol{v}\rangle_\Omega, \end{aligned}$$

where $\langle\cdot,\cdot\rangle$ represents the duality pairing between V and its dual V′. Assuming that the load function $\boldsymbol{f}$ belongs to V′, we can express (6) in the following form: Find $(\boldsymbol{u}, p) \in \mathrm{V}\times\Pi$, such that

$$\begin{aligned} \boldsymbol{A}(\boldsymbol{u}, \boldsymbol{v}) + \boldsymbol{B}(\boldsymbol{v}, p) + \boldsymbol{c}(\boldsymbol{u}; \boldsymbol{u}, \boldsymbol{v}) = \mathcal{F}(\boldsymbol{v}) \quad & \forall\boldsymbol{v} \in \mathrm{V}, \\ \boldsymbol{B}(\boldsymbol{u}, q) = 0 \qquad & \forall q \in \Pi, \end{aligned} \tag{7}$$

where

$$\begin{aligned} \boldsymbol{A}(\boldsymbol{u}, \boldsymbol{v}) &\coloneqq \boldsymbol{a}(\boldsymbol{u}, \boldsymbol{v}) + \boldsymbol{a}^\partial_\tau(\boldsymbol{u}, \boldsymbol{v}), \\ \boldsymbol{B}(\boldsymbol{v}, p) &\coloneqq \boldsymbol{b}(\boldsymbol{v}, p), \end{aligned} \tag{8}$$

with forms defined so that

$$\begin{aligned}
\boldsymbol{a}(\boldsymbol{u},\boldsymbol{v}) &\coloneqq \frac{\nu}{2}(D(\boldsymbol{u}),D(\boldsymbol{v}))_\Omega,\\
\boldsymbol{b}(\boldsymbol{v},p) &\coloneqq -(\operatorname{div}\boldsymbol{v},p)_\Omega,\\
\boldsymbol{a}_\tau^\partial(\boldsymbol{u},\boldsymbol{v}) &\coloneqq \int_{\Gamma_{\mathrm{Nav}}}\beta\sum_i^{d-1}\left(\boldsymbol{\tau}^i\cdot\boldsymbol{u}\right)\left(\boldsymbol{\tau}^i\cdot\boldsymbol{v}\right)\mathrm{d}s,\\
\boldsymbol{c}(\boldsymbol{w};\boldsymbol{u},\boldsymbol{v}) &\coloneqq (\boldsymbol{w}\cdot\nabla\boldsymbol{u},\boldsymbol{v})_\Omega,\\
\mathcal{F}(\boldsymbol{v}) &\coloneqq \langle\boldsymbol{f},\boldsymbol{v}\rangle_\Omega.
\end{aligned}$$

The derivation of the weak formulation is detailed in [31]. In what remains of this section, we will establish the continuity, ellipticity, and inf-sup properties of some operators that will be instrumental for our analysis ahead.

Lemma 1. *There exist positive constants C_1, C_2, and C_3 such that*

$$\begin{aligned}
|\boldsymbol{A}(\boldsymbol{u},\boldsymbol{v})| &\le C_1\|\boldsymbol{u}\|_{1,\Omega}\|\boldsymbol{v}\|_{1,\Omega} && \forall\boldsymbol{u},\boldsymbol{v}\in\mathrm{V},\\
|\boldsymbol{c}(\boldsymbol{w};\boldsymbol{u},\boldsymbol{v})| &\le C_2\|\boldsymbol{w}\|_{1,\Omega}\|\boldsymbol{u}\|_{1,\Omega}\|\boldsymbol{v}\|_{1,\Omega} && \forall\boldsymbol{u},\boldsymbol{v},\boldsymbol{w}\in\mathrm{V},\\
|\boldsymbol{B}(\boldsymbol{v},p)| &\le C_3\|\boldsymbol{v}\|_{1,\Omega}\|p\|_{0,\Omega} && \forall\boldsymbol{v}\in\mathrm{V},p\in\Pi,\\
|\mathcal{F}(\boldsymbol{v})| &\le \|\boldsymbol{f}\|_{\mathrm{V}'}\|\boldsymbol{v}\|_{\mathrm{V}} && \forall\boldsymbol{v}\in\mathrm{V}.
\end{aligned}$$

Proof. These inequalities are a direct consequence of (1), (2), (3), Cauchy–Schwarz and Hölder's inequalities. The constants C_1, C_2, and C_3 depend on the domain Ω, ν and β and it can be seen that

$$\begin{aligned}
C_1 &= \max\left\{\frac{\nu}{2},\beta\right\},\\
C_2 &= C_{\mathrm{Sob}}(q,n),\\
C_3 &= 1.
\end{aligned}$$

□

Let Z be the kernel of $\boldsymbol{B}$, that is

$$\mathrm{Z}\coloneqq\{\boldsymbol{v}\in\mathrm{V}:\boldsymbol{B}(\boldsymbol{v},p)=0,\quad\forall p\in\Pi\}=\{\boldsymbol{v}\in\mathrm{V}:(\operatorname{div}\boldsymbol{v},p)=0,\ \ \forall p\in\Pi\}.$$

It can be rewritten as:

$$\mathrm{Z}\coloneqq\{\boldsymbol{v}\in\mathrm{V}:\operatorname{div}\boldsymbol{v}=0\quad\text{in}\,\Omega\}.$$

Lemma 2. *Assume $|\Gamma_D|>0$ and that b satisfies $b>b_0$ for some sufficiently small negative b_0. Then there exists a positive constant C_b such that the following Poincarè type inequality holds:*

$$\int_\Omega|\boldsymbol{v}|^2\,\mathrm{d}\boldsymbol{x}\le C_b\left(\frac{1}{2}\int_\Omega|D(\boldsymbol{v})|^2\,\mathrm{d}\boldsymbol{x}+\int_{\Gamma_{Nav}}b|P_T\boldsymbol{v}|^2\,\mathrm{d}s\right)\quad\forall\boldsymbol{v}\in\mathrm{Z},\tag{9}$$

where C_b depends on Ω, Γ_{Nav}, and b. It is considered to be the smallest positive constant such that (9) holds and P_T is the projection on the tangent space. For more details on this condition, see [54].

The following lemma establishes the ellipticity of $\boldsymbol{A}$ on Z.

Remark 1. We emphasize that this result allows for negative values of β. For instance (see [31]), in the case of potential flow around a circular cylinder, $\beta=-2$.

Lemma 3. *There exist a constant $\xi > 0$ depends on β, ν, Ω and Γ_{Nav} such that*

$$\boldsymbol{A}(\boldsymbol{v},\boldsymbol{v}) \geq \xi \|\boldsymbol{v}\|_{1,\Omega}^2 \qquad \forall \boldsymbol{v} \in \mathrm{Z}, \tag{10}$$

where $\xi = \min\{\frac{\nu}{2}, \frac{\nu}{4C_{4\beta/\nu}}\}$ and $C_{4\beta/\nu}$ is the constant C_b from Lemma 2 with $b = 4\beta/\nu$.

Proof. Consider the bilinear form

$$\boldsymbol{A}(\boldsymbol{v},\boldsymbol{v}) = \frac{\nu}{2}(D(\boldsymbol{v}), D(\boldsymbol{v}))_\Omega + \int_{\Gamma_{\mathrm{Nav}}} \beta \sum_i^{d-1} \big(\boldsymbol{\tau}^i \cdot \boldsymbol{v}\big)\big(\boldsymbol{\tau}^i \cdot \boldsymbol{v}\big)\,\mathrm{d}s.$$

By introducing the tangent space T and the projection P_T onto the tangent space, allows the boundary term to be expressed in coordinate free form *i.e.*, $P_T = I - \boldsymbol{n} \otimes \boldsymbol{n}$ [66]. Then

$$\sum_{i=1}^{d-1} \big(\boldsymbol{\tau}^i \cdot \boldsymbol{v}\big)\big(\boldsymbol{\tau}^i \cdot \boldsymbol{u}\big) = (P_T\boldsymbol{v}) \cdot (P_T\boldsymbol{u}),$$

and also we use the Lemma 2 as follows:

$$\begin{aligned}
\boldsymbol{A}(\boldsymbol{v},\boldsymbol{v}) &= \frac{\nu}{2}\int_\Omega |D(\boldsymbol{v})|^2\,\mathrm{d}\boldsymbol{x} + \int_{\Gamma_{\mathrm{Nav}}} \beta |P_T\boldsymbol{v}|^2\,\mathrm{d}s \\
&= \frac{\nu}{4}\int_\Omega |D(\boldsymbol{v})|^2\,\mathrm{d}\boldsymbol{x} + \frac{\nu}{4}\left(\int_\Omega |D(\boldsymbol{v})|^2\,\mathrm{d}\boldsymbol{x} + \int_{\Gamma_{\mathrm{Nav}}} \frac{4\beta}{\nu}|P_T\boldsymbol{v}|^2\,\mathrm{d}s\right) \\
&\geq \frac{\nu}{4}\int_\Omega |D(\boldsymbol{v})|^2\,\mathrm{d}\boldsymbol{x} + \frac{\nu}{4C_{4\beta/\nu}}\int_\Omega |\boldsymbol{v}|^2\,\mathrm{d}\boldsymbol{x} \\
&\geq \xi\|\boldsymbol{v}\|_{1,\Omega}^2 \quad \forall \boldsymbol{v} \in \mathrm{Z}.
\end{aligned}$$

where $\xi = \min\{\frac{\nu}{2}, \frac{\nu}{4C_{4\beta/\nu}}\}$. The constant C_b depends on Ω, Γ_{Nav} and b, but given that the geometry is fixed, we denote the dependence only on b. Interestingly, it was shown in [32] that the function $b \mapsto C_b$ is monotone decreasing. □

Next, we present the continuous inf-sup condition for the bilinear form $\boldsymbol{B}$.

Lemma 4. *There exist a positive constant $\theta > 0$ dependent on the shape of the domain Ω such that*

$$\sup_{\boldsymbol{0}\neq\boldsymbol{v}\in\mathrm{V}} \frac{|\boldsymbol{B}(\boldsymbol{v},q)|}{\|\boldsymbol{v}\|_{1,\Omega}} \geq \theta\|q\|_{0,\Omega} \qquad \forall q \in \Pi. \tag{11}$$

Proof. See [30] for a proof. □

2.2.1. The fixed point operator

In this section, we assume that the data is sufficiently small and utilize the Banach fixed point theorem to establish the existence and uniqueness of a solution for equation (7). Let us introduce the bounded set

$$\boldsymbol{K} := \big\{\boldsymbol{v} \in \mathrm{V} : \|\boldsymbol{v}\|_{1,\Omega} \leq \alpha^{-1}\|\boldsymbol{f}\|_{\mathrm{V}'}\big\}, \tag{12}$$

with α is a positive constant defined in (18). Now, we define the fixed point operator as

$$\mathcal{J} : \boldsymbol{K} \to \boldsymbol{K}, \quad \mathrm{d}\boldsymbol{w} \to \mathcal{J}(\boldsymbol{w}) = \boldsymbol{u}, \tag{13}$$

where given $\boldsymbol{w} \in \boldsymbol{K}$, $\boldsymbol{u}$ is the first component of the solution of the linearised version of problem (7): Find $(\boldsymbol{u}, p) \in \mathrm{V} \times \Pi$, such that

$$\begin{aligned} \boldsymbol{A}(\boldsymbol{u},\boldsymbol{v}) + \boldsymbol{B}(\boldsymbol{v},p) + \boldsymbol{c}(\boldsymbol{w};\boldsymbol{u},\boldsymbol{v}) &= \mathcal{F}(\boldsymbol{v}) \qquad \forall \boldsymbol{v} \in \mathrm{V}, \\ \boldsymbol{B}(\boldsymbol{u},q) &= 0 \qquad \forall q \in \Pi. \end{aligned} \tag{14}$$

Based on the above, we establish the following relation

$$\mathcal{J}(\boldsymbol{u}) = \boldsymbol{u} \Leftrightarrow (\boldsymbol{u},p) \in \mathrm{V} \times \Pi \text{ satisfies (7)}. \tag{15}$$

Therefore, to demonstrate the well-posedness of (7), it is sufficient to prove that the fixed point operator $\mathcal{J}$ possesses a unique fixed point. Let us now introduce the bilinear form as

$$\mathcal{C}[(\boldsymbol{u},p);(\boldsymbol{v},q)] = \boldsymbol{A}(\boldsymbol{u},\boldsymbol{v}) + \boldsymbol{B}(\boldsymbol{u},q) + \boldsymbol{B}(\boldsymbol{v},p). \tag{16}$$

Lemma 5. *There exist a positive constant α such that*

$$\sup_{\boldsymbol{0} \neq (\boldsymbol{u},p) \in \mathrm{V} \times \Pi} \frac{\mathcal{C}[(\boldsymbol{u},p);(\boldsymbol{v},q)]}{\|\boldsymbol{v},q)\|} \geq \alpha \|(\boldsymbol{u},p)\| \qquad \forall (\boldsymbol{u},p) \in \mathrm{V} \times \Pi, \tag{17}$$

with

$$\alpha = \xi\theta \min\left\{\frac{1}{\xi+\theta+1}, \frac{\theta}{(\xi+1)(\theta+1)}\right\}, \tag{18}$$

where ξ and θ are the coercivity and inf-sup stability constants respectively.

Proof. Proposition 2.36 from [26] in which Lemmas 3 and 4 are used. □

It is possible to establish the well-posedness of $\mathcal{J}$ and thus the unisolvence of (7). These results are well-established, so we report them without proof.

Theorem 1. *Assume that*

$$\frac{2}{\alpha^2}\|\boldsymbol{f}\|_{\mathrm{V}'} \leq 1. \tag{19}$$

Then, given $\boldsymbol{w} \in \boldsymbol{K}$, there exists a unique $\boldsymbol{u} \in \boldsymbol{K}$ such that $\mathcal{J}(\boldsymbol{w}) = \boldsymbol{u}$.

Theorem 2. *Let $\boldsymbol{f} \in \mathrm{V}'$ such that*

$$\frac{2}{\alpha^2}\|\boldsymbol{f}\|_{\mathrm{V}'} \leq 1. \tag{20}$$

Then, there exists a unique $(\boldsymbol{u},p) \in \mathrm{V} \times \Pi$ solution to (7). In addition, there exists a positive constant $C(\nu,\beta,\Omega) = \max\{\frac{2}{\alpha}, \frac{1}{\alpha}\}$ such that

$$\|\boldsymbol{u}\|_1 + \|p\|_{0,\Omega} \leq C\|\boldsymbol{f}\|_{\mathrm{V}'}. \tag{21}$$

3. Discrete problem

This section studies the solvability and convergence analysis of Nitsche's scheme for the problem (7). We assume that the polygonal computational domain Ω is discretized using a collection of regular partitions, denoted as $\{\mathcal{K}_h\}_{h>0}$, where $\Omega \subset \mathbb{R}^d$ is divided into simplices K (triangles in 2D or tetrahedra in 3D) with a diameter h_K. The characteristic length of the finite element mesh $\mathcal{K}_h$ is denoted as $h := \max_{K\in\mathcal{K}_h} h_K$. For a given triangulation $\mathcal{K}_h$, we define $\mathcal{E}_h$ as the set of all faces in $\mathcal{K}_h$, with the following partitioning

$$\mathcal{E}_h := \mathcal{E}_\Omega \cup \mathcal{E}_D \cup \mathcal{E}_{\mathrm{Nav}}$$

where $\mathcal{E}_\Omega$ represents the faces lying in the interior of Ω, $\mathcal{E}_{\mathrm{Nav}}$ represents the faces lying on the boundary Γ_{Nav}, and $\mathcal{E}_D$ represents the faces lying on the boundary Γ_D. Additionally, h_e denotes the $(d-1)$ dimensional diameter of a face. Here *faces* loosely refers to the geometrical entities of co-dimension 1. Now, let us introduce the finite element pair.

$$\begin{aligned}
\mathrm{V}_h &:= \left\{\boldsymbol{v}_h \in \boldsymbol{C}(\overline{\Omega}) : \boldsymbol{v}_h = 0 \ \text{ on } \ E \in \mathcal{E}_D, \boldsymbol{v}_h|_K \in \mathbb{P}_k(K) \quad \forall K \in \mathcal{K}_h\right\},\\
\Pi_h &:= \left\{q_h \in \mathrm{C}(\overline{\Omega}) : q_h|_K \in \mathbb{P}_{k-1}(K) \quad \forall K \in \mathcal{K}_h\right\} \cap \Pi,
\end{aligned}$$

where $\mathbb{P}_k(K)$ is the space of polynomials of degree less than or equal to k defined on K.

Remark 2. It is noted that Π_h is a subspace of Π, but V_h is not a subspace of V. In that sense, Nitsche's method can be considered a non-conforming finite element approximation.

3.1. Nitsche's method

The main objective of Nitsche's method [57, 66] is to impose boundary conditions weakly so that they hold only asymptotically, which for this work will hold for the Navier boundary condition $\boldsymbol{u}\cdot\boldsymbol{n} = 0$ only. As a result, the weak formulation with the symmetric variant of the Nitsche method can be expressed as follows: Find $(\boldsymbol{u}_h, p_h) \in \mathrm{V}_h \times \Pi_h$, such that

$$\mathcal{A}_h[(\boldsymbol{u}_h, p_h); (\boldsymbol{v}_h, q_h)] = \mathcal{F}(\boldsymbol{v}_h) \quad \forall(\boldsymbol{v}_h, q_h) \in \mathrm{V}_h \times \Pi_h, \tag{22}$$

with the forms are defined as

$$\begin{aligned}
\mathcal{A}_h[(\boldsymbol{u}_h, p_h); (\boldsymbol{v}_h, q_h)] &:= \sum_{K\in\mathcal{K}_h}\Big(\frac{\nu}{2}(D(\boldsymbol{u}_h), D(\boldsymbol{v}_h))_K + (\boldsymbol{u}_h\cdot\nabla\boldsymbol{u}_h, \boldsymbol{v}_h)_K - (p_h, \nabla\cdot\boldsymbol{v}_h)_K - (q_h, \nabla\cdot\boldsymbol{u}_h)_K\Big)\\
&\quad + \sum_{E\in\mathcal{E}_{\mathrm{Nav}}}\Big(-\int_E \boldsymbol{n}^t(\nu D(\boldsymbol{u}_h) - p_h I)\boldsymbol{n}(\boldsymbol{n}\cdot\boldsymbol{v}_h)\,\mathrm{d}s - \int_E \boldsymbol{n}^t(\nu D(\boldsymbol{v}_h) - q_h I)\boldsymbol{n}(\boldsymbol{n}\cdot\boldsymbol{u}_h)\,\mathrm{d}s\\
&\quad + \int_E \beta\sum_i^{d-1}(\boldsymbol{\tau}^i\cdot\boldsymbol{v}_h)(\boldsymbol{\tau}^i\cdot\boldsymbol{u}_h)\,\mathrm{d}s + \gamma\int_E {h_e}^{-1}(\boldsymbol{u}_h\cdot\boldsymbol{n})(\boldsymbol{v}_h\cdot\boldsymbol{n})\,\mathrm{d}s\Big),\\
\mathcal{F}(\boldsymbol{v}_h) &:= \langle \boldsymbol{f}, \boldsymbol{v}_h\rangle,
\end{aligned}$$

and $\gamma > 0$ is a positive constant that needs to be chosen sufficiently large, as proved in Lemma 8 later. We can rewrite (22) as: Find $(\boldsymbol{u}_h, p_h) \in \mathrm{V}_h \times \Pi_h$, such that

$$\begin{aligned}
\boldsymbol{A}_h(\boldsymbol{u}_h, \boldsymbol{v}_h) + \boldsymbol{B}_h(\boldsymbol{v}_h, p_h) + \boldsymbol{c}(\boldsymbol{u}_h; \boldsymbol{u}_h, \boldsymbol{v}_h) &= \mathcal{F}(\boldsymbol{v}_h) \qquad \forall \boldsymbol{v}_h \in \mathrm{V}_h,\\
\boldsymbol{B}_h(\boldsymbol{u}_h, q_h) &= 0 \qquad\quad\ \ \forall q_h \in \Pi_h,
\end{aligned}\tag{23}$$

where

$$\begin{aligned}
\boldsymbol{A}_h(\boldsymbol{u}_h, \boldsymbol{v}_h) &:= \boldsymbol{a}(\boldsymbol{u}_h, \boldsymbol{v}_h) + \boldsymbol{a}^\partial_\tau(\boldsymbol{u}_h, \boldsymbol{v}_h) + \boldsymbol{a}^\partial_\gamma(\boldsymbol{u}_h, \boldsymbol{v}_h) - \boldsymbol{a}^\partial_c(\boldsymbol{u}_h, \boldsymbol{v}_h) - \boldsymbol{a}^\partial_c(\boldsymbol{v}_h, \boldsymbol{u}_h),\\
\boldsymbol{B}_h(\boldsymbol{u}_h, q_h) &:= \boldsymbol{b}(\boldsymbol{u}_h, q_h) + \boldsymbol{b}^\partial(\boldsymbol{u}_h, q_h),
\end{aligned}\tag{24}$$

with forms defined so that

$$\begin{aligned}
\boldsymbol{a}(\boldsymbol{u}_h, \boldsymbol{v}_h) &\coloneqq \sum_{K\in\mathcal{K}_h} \frac{\nu}{2}\big(D(\boldsymbol{u}_h), D(\boldsymbol{v}_h)\big)_K,\\
\boldsymbol{b}(\boldsymbol{u}_h, q_h) &\coloneqq -\sum_{K\in\mathcal{K}_h} (\operatorname{div}\boldsymbol{u}_h, q_h)_K,\\
\boldsymbol{b}^\partial(\boldsymbol{u}_h, q_h) &\coloneqq \sum_{E\in\mathcal{E}_{\mathrm{Nav}}} \int_E q_h(\boldsymbol{n}\cdot\boldsymbol{u}_h)\,\mathrm{d}s,\\
\boldsymbol{a}_c^\partial(\boldsymbol{u}_h, \boldsymbol{v}_h) &\coloneqq \sum_{E\in\mathcal{E}_{\mathrm{Nav}}} \int_E \boldsymbol{n}^t\nu D(\boldsymbol{u}_h)\boldsymbol{n}(\boldsymbol{n}\cdot\boldsymbol{v}_h)\,\mathrm{d}s,\\
\boldsymbol{a}_\tau^\partial(\boldsymbol{u}_h, \boldsymbol{v}_h) &\coloneqq \sum_{E\in\mathcal{E}_{\mathrm{Nav}}} \int_E \beta\sum_i^{d-1}\big(\boldsymbol{\tau}^i\cdot\boldsymbol{u}_h\big)\big(\boldsymbol{\tau}^i\cdot\boldsymbol{v}_h\big)\,\mathrm{d}s,\\
\boldsymbol{a}_\gamma^\partial(\boldsymbol{u}_h, \boldsymbol{v}_h) &\coloneqq \sum_{E\in\mathcal{E}_{\mathrm{Nav}}} \int_E \frac{\gamma}{h_e}(\boldsymbol{u}_h\cdot\boldsymbol{n})(\boldsymbol{v}_h\cdot\boldsymbol{n})\,\mathrm{d}s,\\
\mathcal{F}(\boldsymbol{v}_h) &\coloneqq \langle\boldsymbol{f}, \boldsymbol{v}_h\rangle,\\
\boldsymbol{c}(\boldsymbol{w}_h; \boldsymbol{u}_h, \boldsymbol{v}_h) &\coloneqq \sum_{K\in\mathcal{K}_h} (\boldsymbol{w}_h\cdot\nabla\boldsymbol{u}_h, \boldsymbol{v}_h)_K.
\end{aligned} \tag{25}$$

We note that the terms that appear for the slip boundary condition, *i.e.*, the ones with the ∂ superscript, can be used also within a RANS framework, as the treatment of boundary conditions is identical.

3.1.1. Discrete stability properties

In this section, we leverage well-known inverse and trace inequalities to establish two results: the ellipticity of $\boldsymbol{A}_h$ and the inf-sup property $\boldsymbol{B}_h$.

Lemma 6. *Let $\boldsymbol{v}_h \in \mathrm{V}_h$ then for each $K \in \mathcal{K}_h$; $l, m \in \mathbb{N}$, with $0 \le m \le l$, there exists a positive constant C_4, independent of K, such that*

$$|\boldsymbol{v}_h|_{l,K} \le C_4 h_K^{m-l}|\boldsymbol{v}_h|_{m,K}.$$

Proof. Lemma 12.1 from [26]. ☐

Lemma 7. *Let $\boldsymbol{v}_h \in \mathrm{V}_h$ then for each $K \in \mathcal{K}_h, E \subset \partial K$, there exists a positive constant C_5, independent of K, such that*

$$\|\boldsymbol{v}_h\|_{0,E} \le C_5 h_K^{-\frac{1}{2}}\|\boldsymbol{v}_h\|_{0,K}.$$

Proof. See [65]. ☐

We need to define the energy norm on V_h as

$$\|\boldsymbol{v}_h\|_{1,h}^2 \coloneqq \|\nabla\boldsymbol{v}_h\|_{0,\Omega}^2 + \sum_{E\in\mathcal{E}_{\mathrm{Nav}}} \frac{1}{h_e}\|\boldsymbol{v}_h\cdot\boldsymbol{n}\|_{0,E}^2. \tag{26}$$

In contrast to the one found in [2], we highlight that this norm contains only those boundary terms that correspond to normal components because we impose only the Navier boundary condition weakly in the weak formulation. Still, our proof would remain mostly unmodified if we also weakly considered the Dirichlet boundary conditions. We would only require adding the missing velocity for this energy norm. All estimates would remain the same. We now state the continuity of the discrete bilinear forms in this norm.

Theorem 3. *There exist positive constants C_7, C_8, and C_9 independent of h such that*

$$\begin{aligned} |\boldsymbol{A}_h(\boldsymbol{u}_h,\boldsymbol{v}_h)| &\le C_7\|\boldsymbol{u}_h\|_{1,h}\|\boldsymbol{v}_h\|_{1,h}, && \forall \boldsymbol{u}_h,\boldsymbol{v}_h \in \mathrm{V}_h,\\ |\boldsymbol{c}(\boldsymbol{w}_h;\boldsymbol{u}_h,\boldsymbol{v}_h)| &\le C_8\|\boldsymbol{w}_h\|_{1,h}\|\boldsymbol{u}\|_{1,h}\|\boldsymbol{v}_h\|_{1,h}, && \forall \boldsymbol{w}_h,\boldsymbol{u}_h,\boldsymbol{v}_h \in \mathrm{V}_h,\\ |\boldsymbol{B}_h(\boldsymbol{v}_h,q_h)| &\le C_9\|\boldsymbol{v}_h\|_{1,h}\|q_h\|_{0,\Omega}, && \forall \boldsymbol{v}_h \in \mathrm{V}_h, q_h\in \Pi_h. \end{aligned}$$

Proof. The proof of the above inequalities is a direct consequence of Lemmas 6 and 7, Sobolev embedding with $r=4$, Cauchy–Schwarz and Hölder inequalities. Moreover, it can be seen that

$$\begin{aligned} C_7 &= \frac{\nu}{2}+\beta+\gamma+\nu C_5,\\ C_8 &= C_{\mathrm{Sob}}(4,n),\\ C_9 &= 1+C_5, \end{aligned}$$

i.e., the above constants can bounded by a constant that depends only on the trace inequality constant C_5, and on the parameters ν ,γ, and β. □

The discrete kernel of $\boldsymbol{B}_h$ is defined by:

$$\mathrm{Z}_h := \{\boldsymbol{v}_h \in \mathrm{V}_h : \boldsymbol{B}_h(\boldsymbol{v}_h,p_h)=0, \forall p_h\in\Pi_h\}.$$

It can be equivalently written as

$$\mathrm{Z}_h := \left\{\boldsymbol{v}_h \in \mathrm{V}_h : \sum_{K\in\mathcal{K}_h}\int_K p_h\nabla\cdot\boldsymbol{v}_h\,\mathrm{d}\boldsymbol{x} - \sum_{E\in\mathcal{E}_{\mathrm{Nav}}}\int_E p_h(\boldsymbol{n}\cdot\boldsymbol{v}_h)\,\mathrm{d}s = 0 \quad \forall p_h\in\Pi_h\right\}. \tag{27}$$

The following lemma establishes the ellipticity of $\boldsymbol{A}$ on V_h.

Lemma 8. *There exist positive constants γ_0, C_0 and $C_S = C_S(\beta,\nu,\Omega)$, independent on h, such that*

$$\boldsymbol{A}_h(\boldsymbol{v}_h,\boldsymbol{v}_h) \ge C_S\|\boldsymbol{v}_h\|^2_{1,h} \quad \forall \boldsymbol{v}_h\in \mathrm{Z}_h, \tag{28}$$

where $C_S=\min\{\xi-\nu C_5^2 C_0, \gamma-\frac{\nu}{C_0}\}$ with $\gamma\ge\gamma_0>\frac{\nu}{C_0}$, $C_0<\frac{\xi}{C_5^2\nu}$, and ξ is the coercivity constant defined in the continuous case.

Proof. For the proof, we use (24) to obtain

$$\begin{aligned} \boldsymbol{A}_h(\boldsymbol{v}_h,\boldsymbol{v}_h) = \frac{\nu}{2}(D(\boldsymbol{v}_h),D(\boldsymbol{v}_h))_\Omega &+ \sum_{E\in\mathcal{E}_{\mathrm{Nav}}}\int_E \beta\sum_{i}^{d-1}(\boldsymbol{\tau}^i\cdot\boldsymbol{v}_h)(\boldsymbol{\tau}^i\cdot\boldsymbol{v}_h)\,\mathrm{d}s\\ &- \sum_{E\in\mathcal{E}_{\mathrm{Nav}}} 2\int_E \boldsymbol{n}^t\nu D(\boldsymbol{v}_h)\boldsymbol{n}(\boldsymbol{n}\cdot\boldsymbol{v}_h)\,\mathrm{d}s + \frac{\gamma}{h_e}\int_E(\boldsymbol{v}_h\cdot\boldsymbol{n})(\boldsymbol{v}_h\cdot\boldsymbol{n})\,\mathrm{d}s. \end{aligned}$$

Using Lemmas 3 and 7, Cauchy–Schwarz and Hölder's inequalities, the following estimate can be established

$$
\begin{aligned}
\boldsymbol{A}_h(\boldsymbol{v}_h,\boldsymbol{v}_h) &\geq \xi\|\nabla \boldsymbol{v}_h\|_{0,\Omega}^2 - 2\nu \sum_{E\in\mathcal{E}_{\mathrm{Nav}}} \|\boldsymbol{v}_h\cdot\boldsymbol{n}\|_{0,E}\|D\boldsymbol{v}_h\boldsymbol{n}\|_{0,E} + \frac{\gamma}{h_e}\sum_{E\in\mathcal{E}_{\mathrm{Nav}}}\|\boldsymbol{v}_h\cdot\boldsymbol{n}\|_{0,E}^2\\
&\geq \xi\|\nabla \boldsymbol{v}_h\|_{0,\Omega}^2 - 2\nu \sum_{E\in\mathcal{E}_{\mathrm{Nav}}} h_e^{-1/2}\|\boldsymbol{v}_h\cdot\boldsymbol{n}\|_{0,E}h_e^{1/2}\|D\boldsymbol{v}_h\boldsymbol{n}\|_{0,E} + \frac{\gamma}{h_e}\sum_{E\in\mathcal{E}_{\mathrm{Nav}}}\|\boldsymbol{v}_h\cdot\boldsymbol{n}\|_{0,E}^2\\
&\geq \xi\|\nabla \boldsymbol{v}_h\|_{0,\Omega}^2 - 2\nu \sum_{E\in\mathcal{E}_{\mathrm{Nav}}} \left(\frac{h_eC_0}{2}\|D\boldsymbol{v}_h\|_{0,E}^2 + \frac{h_e^{-1}}{2C_0}\|\boldsymbol{v}_h\cdot\boldsymbol{n}\|_{0,E}^2\right) + \frac{\gamma}{h_e}\sum_{E\in\mathcal{E}_{\mathrm{Nav}}}\|\boldsymbol{v}_h\cdot\boldsymbol{n}\|_{0,E}^2\\
&\geq \xi\|\nabla \boldsymbol{v}_h\|_{0,\Omega}^2 - \nu C_5^2C_0 \sum_{K\in\mathcal{T}_h}\|D\boldsymbol{v}_h\|_{0,K}^2 - \frac{\nu}{C_0\gamma}\sum_{E\in\mathcal{E}_{\mathrm{Nav}}}\frac{\gamma}{h_e}\|\boldsymbol{v}_h\cdot\boldsymbol{n}\|_{0,E}^2 + \frac{\gamma}{h_e}\sum_{E\in\mathcal{E}_{\mathrm{Nav}}}\|\boldsymbol{v}_h\cdot\boldsymbol{n}\|_{0,E}^2\\
&\geq \xi\|\nabla \boldsymbol{v}_h\|_{0,\Omega}^2 - \nu C_5^2C_0\|\nabla \boldsymbol{v}_h\|_{0,\Omega}^2 + \left(1-\frac{\nu}{C_0\gamma}\right)\sum_{E\in\mathcal{E}_{\mathrm{Nav}}}\frac{\gamma}{h_e}\|\boldsymbol{v}_h\cdot\boldsymbol{n}\|_0^2\\
&\geq \left(\xi-\nu C_5^2C_0\right)\|\nabla \boldsymbol{v}_h\|_{0,\Omega}^2 + \left(\gamma-\frac{\nu}{C_0}\right)\sum_{E\in\mathcal{E}_{\mathrm{Nav}}}\frac{1}{h_e}\|\boldsymbol{v}_h\cdot\boldsymbol{n}\|_{0,E}^2\\
&\geq C_S\|\boldsymbol{v}_h\|_{1,h}^2.
\end{aligned}
$$

By selecting the positive parameter C_0 that satisfies $C_0 < \frac{\xi}{C_5^2\nu}$, we ensure that $(\xi - \nu C_5^2 C_0) > 0$. Additionally, we define $C_S = \min\{\xi - \nu C_5^2 C_0, \gamma - \frac{\nu}{C_0}\}$ with $\gamma \geq \gamma_0 > \frac{\nu}{C_0}$. □

Next, we proceed to derive the discrete version of Lemma 4.

Remark 3. The inf-sup condition is associated with the construction of inf-sup stable element in an incompressible flow modeling. However, this condition is not automatically fulfilled and needs to be verified for specific choices of the approximation spaces V_h and Π_h. It is worth mentioning that the Taylor-Hood element are inf-sup stable, meaning they meet the necessary conditions for stability. The proof can be demonstrated using any pair of inf-sup stable element.

Lemma 9. *There exists $\hat{\theta} > 0$ independent of h such that*

$$
\sup_{\mathbf{0}\neq \boldsymbol{v}_h\in\mathrm{V}_h}\frac{|\boldsymbol{B}_h(\boldsymbol{v}_h,q_h)|}{\|\boldsymbol{v}_h\|_{1,h}} \geq \hat{\theta}\|q_h\|_{0,\Omega} \quad \forall q\in\Pi_h. \tag{29}
$$

Proof. Consider the Taylor–Hood Finite element spaces $\mathrm{V}_h\times\Pi_h$ such that the discrete inf-sup holds for the bilinear form $\boldsymbol{b}(\boldsymbol{v}_h, q_h)$, see Section 5.5 from [25] *i.e.*, there exist a positive constant $\hat{\theta} > 0$, independent of h such that

$$
\sup_{\mathbf{0}\neq \boldsymbol{v}_h\in\mathrm{V}_h}\frac{|\boldsymbol{b}(\boldsymbol{v}_h,q_h)|}{\|\boldsymbol{v}_h\|_{1,\Omega}} \geq \hat{\theta}\|q_h\|_{0,\Omega} \qquad \forall q_h\in\Pi_h.
$$

Consider the discrete space of strongly imposed Navier conditions

$$
\mathrm{V}_{h,0} = \{\boldsymbol{v}_h\in\mathrm{V}_h : \boldsymbol{v}_h\cdot\boldsymbol{n} = 0 \text{ on } \Gamma_{\mathrm{Nav}}\}.
$$

This space naturally yields that $b^{\partial}(\boldsymbol{v}_h, q_h) = 0$ for all $\boldsymbol{v}_h$ in $\mathrm{V}_{h,0}$, so we obtain

$$
\sup_{\mathbf{0}\neq \boldsymbol{v}_h\in\mathrm{V}_{h,0}}\frac{|\boldsymbol{B}_h(\boldsymbol{v}_h,q_h)|}{\|\boldsymbol{v}_h\|_{1,h}} = \sup_{\mathbf{0}\neq \boldsymbol{v}_h\in\mathrm{V}_{h,0}}\frac{|\boldsymbol{b}(\boldsymbol{v}_h,q_h)|}{\|\boldsymbol{v}_h\|_{1,h}} = \sup_{\mathbf{0}\neq \boldsymbol{v}_h\in\mathrm{V}_{h,0}}\frac{|\boldsymbol{b}(\boldsymbol{v}_h,q_h)|}{\|\boldsymbol{v}_h\|_{1,\Omega}} \geq \hat{\theta}\|q_h\|_{0,\Omega} \qquad \forall q_h\in\Pi_h
$$

in virtue of the classical inf-sup condition. Now, use this space for a lower bound:

$$\sup_{\mathbf{0}\neq \boldsymbol{v}_h\in \mathrm{V}_h} \frac{|\boldsymbol{B}_h(\boldsymbol{v}_h,q_h)|}{\|\boldsymbol{v}_h\|_{1,h}} \geq \sup_{\mathbf{0}\neq \boldsymbol{v}_h\in \mathrm{V}_{h,0}} \frac{|\boldsymbol{B}_h(\boldsymbol{v}_h,q_h)|}{\|\boldsymbol{v}_h\|_{1,h}} \geq \hat{\theta}\|q_h\|_{0,\Omega} \qquad \forall q_h\in \Pi_h.$$

This concludes the proof. □

Next, we aim to establish the well-posedness of problem (23). We will utilize a fixed-point operator linked to a linearised form of the problem and demonstrate that this operator has a unique fixed point. We can prove the well-posedness of problem (23) using the Banach fixed-point theorem.

3.1.2. The discrete fixed-point operator and its well-posedness

Let us introduce the set

$$\boldsymbol{K_h} := \left\{\boldsymbol{v}_h\in \mathrm{V}_h : \|\boldsymbol{v}_h\|_{1,h}\leq \hat{\alpha}^{-1}\|\boldsymbol{f}\|_{\mathrm{V}'}\right\}, \tag{30}$$

with $\hat{\alpha}>0$ being the constant defined below in Theorem 4. Now, let us define the discrete fixed point operator as

$$\mathcal{J}_h : \boldsymbol{K}_h \to \boldsymbol{K}_h, \quad \mathrm{d}\boldsymbol{w}_h \to \mathcal{J}_h(\boldsymbol{w}_h) = \boldsymbol{u}_h,$$

where given $\boldsymbol{w}_h\in \boldsymbol{K}_h, \boldsymbol{u}_h$ represents the first component of the solution of the linearised version of problem (24): Find $(\boldsymbol{u}_h,p_h)\in \mathrm{V}_h\times \Pi_h$

$$\begin{aligned} \boldsymbol{A}_h(\boldsymbol{u}_h,\boldsymbol{v}_h)+\boldsymbol{B}_h(\boldsymbol{v}_h,p_h)+\boldsymbol{c}(\boldsymbol{w}_h;\boldsymbol{u}_h,\boldsymbol{v}_h) &= \mathcal{F}(\boldsymbol{v}_h) \qquad &&\forall \boldsymbol{v}_h\in \mathrm{V}_h,\\ \boldsymbol{B}_h(\boldsymbol{u}_h,q_h) &= 0 &&\forall q_h\in \Pi_h. \end{aligned} \tag{31}$$

Based on the above, we can establish the following relation

$$\mathcal{J}_h(\boldsymbol{u}_h)=\boldsymbol{u}_h \Leftrightarrow (\boldsymbol{u}_h,p_h)\in \mathrm{V}_h\times \Pi_h \quad \text{satisfies (24)}. \tag{32}$$

To guarantee the well-posedness of the discrete problem (24), it is enough to demonstrate the existence of a unique fixed-point for $\mathcal{J}_h$ within the set $\boldsymbol{K}_h$. However, before delving into the solvability analysis, we first need to establish that operator $\mathcal{J}_h$ is well-defined. Let us introduce the bilinear form.

$$\mathcal{C}_h[(\boldsymbol{u}_h,p_h);(\boldsymbol{v}_h,q_h)] = \boldsymbol{A}_h(\boldsymbol{u}_h,\boldsymbol{v}_h)+\boldsymbol{B}_h(\boldsymbol{u}_h,q_h)+\boldsymbol{B}_h(\boldsymbol{v}_h,p_h). \tag{33}$$

Theorem 4. *There exist a positive constant $\hat{\alpha}$ such that*

$$\sup_{\mathbf{0}\neq(\boldsymbol{v}_h,q_h)\in \mathrm{V}_h\times\Pi_h} \frac{\mathcal{C}_h[(\boldsymbol{u}_h,p_h);(\boldsymbol{v}_h,q_h)]}{\|(\boldsymbol{v}_h,q_h)\|} \geq \hat{\alpha}\|(\boldsymbol{u}_h,p_h)\| \quad \forall(\boldsymbol{u}_h,p_h)\in \mathrm{V}_h\times\Pi_h,$$

with

$$\hat{\alpha} = C_S\hat{\theta}\min\left\{\frac{1}{C_S+\hat{\theta}+1}, \frac{\hat{\theta}}{(C_S+1)(\hat{\theta}+1)}\right\}.$$

where C_S and $\hat{\theta}$ are the coercivity and inf-sup stability constants.

Proof. Owing to Theorem 3, it is clear that $\mathcal{C}_h[\cdot;\cdot]$ is bounded. Moreover, from Lemmas 8, 9, and Proposition 2.36 from [26], it is not difficult to see that the above inf-sup condition holds. □

Now, we are in position to establish the well-posedness of $\mathcal{J}_\mathrm{h}$.

Theorem 5. *Assume that*

$$\frac{2}{\hat{\alpha}^2}\|\boldsymbol{f}\|_{\mathrm{V}'} \leq 1, \tag{34}$$

Then, given $\boldsymbol{w}_h \in \boldsymbol{K}_h$, there exists a unique $\boldsymbol{u}_h \in \boldsymbol{K}_h$ such that $\mathcal{J}_h(\boldsymbol{w}_h) = \boldsymbol{u}_h$.

Proof. Given $\boldsymbol{w}_h \in \boldsymbol{K}_h$, we begin by defining the bilinear form:

$$\mathcal{A}_{\boldsymbol{w}_h}[(\boldsymbol{u}_h, p_h); (\boldsymbol{v}_h, q_h)] := \mathcal{C}_h[(\boldsymbol{u}_h, p_h); (\boldsymbol{v}_h, q_h)] + \boldsymbol{c}(\boldsymbol{w}_h; \boldsymbol{u}_h, \boldsymbol{v}_h), \tag{35}$$

where $\mathcal{C}_h$ and $\boldsymbol{c}$ are the forms defined in Theorem 4 and (25), respectively, that is

$$\mathcal{A}_{\boldsymbol{w}_h}[(\boldsymbol{u}_h, p_h); (\boldsymbol{v}_h, q_h)] = \boldsymbol{A}_h(\boldsymbol{u}_h, \boldsymbol{v}_h) + \boldsymbol{B}_h(\boldsymbol{u}_h, q_h) + \boldsymbol{B}_h(\boldsymbol{v}_h, q_h) + \boldsymbol{c}(\boldsymbol{w}_h; \boldsymbol{u}_h, \boldsymbol{v}_h).$$

Then, problem (23) can be rewritten equivalently as: Given $\boldsymbol{w}_h$ in $\boldsymbol{K}_h$, find $(\boldsymbol{u}_h, p_h) \in \mathrm{V}_h \times \Pi_h$, such that

$$\mathcal{A}_{\boldsymbol{w}_h}[(\boldsymbol{u}_h, p_h); (\boldsymbol{v}_h, q_h)] = \mathcal{F}(\boldsymbol{v}_h) \quad \forall (\boldsymbol{v}_h, q_h) \in \mathrm{V}_h \times \Pi_h. \tag{36}$$

First, we establish the well-posedness of $\mathcal{J}$ in order to demonstrate the well posedness of problem (36) using the Banach Nečas Babuška theorem ([26], Theorem 2.6). Consider $(\boldsymbol{u}_h, p_h), (\hat{\boldsymbol{v}}_h, \hat{q}_h) \in \mathrm{V}_h \times \Pi_h$ with $(\hat{\boldsymbol{v}}_h, \hat{q}_h) \neq 0$, from Theorem 3 we can observe that

$$\begin{aligned}\sup_{\mathbf{0}\neq(\boldsymbol{v}_h,p_h)\in\mathrm{V}_h\times\Pi_h} \frac{\mathcal{A}_{\boldsymbol{w}_h}[(\boldsymbol{u}_h, p_h); (\boldsymbol{v}_h, q_h)]}{\|(\boldsymbol{v}_h, q_h)\|} &\geq \frac{|\mathcal{C}_h[(\boldsymbol{u}_h, p_h); (\hat{\boldsymbol{v}_h}, \hat{q}_h)]|}{\|(\hat{\boldsymbol{v}_h}, \hat{q}_h)\|} - \frac{|\boldsymbol{c}(\boldsymbol{w}_h; \boldsymbol{u}_h, \hat{\boldsymbol{v}}_h)|}{\|(\hat{\boldsymbol{v}}_h, \hat{q}_h)\|} \\ &\geq \frac{|\mathcal{C}_h[(\boldsymbol{u}_h, p_h); (\hat{\boldsymbol{v}_h}, \hat{q}_h)]|}{\|(\hat{\boldsymbol{v}_h}, \hat{q}_h)\|} - \|\boldsymbol{w}_h\|_{1,h}\|(\boldsymbol{u}_h, p_h)\|,\end{aligned}$$

which together with Theorem 4 and the fact that $(\hat{\boldsymbol{v}}_h, \hat{p}_h)$ is arbitrary, implies

$$\sup_{\mathbf{0}\neq(\boldsymbol{v}_h,p_h)\in\mathrm{V}_h\times\Pi_h} \frac{\mathcal{A}_{\boldsymbol{w}_h}[(\boldsymbol{u}_h, p_h); (\boldsymbol{v}_h, q_h)]}{\|(\boldsymbol{v}_h, p_h)\|} \geq (\hat{\alpha} - \|\boldsymbol{w}_h\|_{1,h})\|(\boldsymbol{u}_h, p_h)\|, \tag{37}$$

where $\hat{\alpha}$ is independent of $\boldsymbol{w}_h$. Hence, from the definition of set $\boldsymbol{K}_h$ see (30), and assumption (34), we easily get

$$\|\boldsymbol{w}_h\|_{1,h} \leq \frac{1}{\hat{\alpha}}\|\boldsymbol{f}\|_{\mathrm{V}'} \leq \frac{\hat{\alpha}}{2}, \tag{38}$$

and then, combining (37) and (38), we obtain

$$\sup_{\mathbf{0}\neq(\boldsymbol{v}_h,p_h)\in\mathrm{V}_h\times\Pi_h} \frac{\mathcal{A}_{\boldsymbol{w}_h}[(\boldsymbol{u}_h, p_h); (\boldsymbol{v}_h, q_h)]}{\|(\boldsymbol{v}_h, q_h)\|} \geq \frac{\hat{\alpha}}{2}\|(\boldsymbol{u}_h, p_h)\| \quad \forall (\boldsymbol{u}_h, p_h) \in \mathrm{V}_h \times \Pi_h. \tag{39}$$

On the other hand, for a given $(\boldsymbol{u}_h, q_h) \in \mathrm{V}_h \times \Pi_h$, we observe that

$$\begin{aligned}\sup_{\mathbf{0}\neq(\boldsymbol{v}_h,q_h)\in\boldsymbol{V}_h\times\Pi_h} \mathcal{A}_{\mathrm{w}_h}[(\boldsymbol{v}_h, q_h); (\boldsymbol{u}_h, p_h)] &\geq \sup_{\mathbf{0}\neq(\boldsymbol{v}_h,q_h)\in\mathrm{V}_h\times\Pi_h} \frac{\mathcal{A}_{\boldsymbol{w}_h}[(\boldsymbol{v}_h, q_h); (\boldsymbol{u}_h, p_h)]}{\|(\boldsymbol{v}_h, q_h)\|} \\ &= \sup_{\mathbf{0}\neq(\boldsymbol{v}_h,q_h)\in\mathrm{V}_h\times\Pi_h} \frac{\mathcal{C}_h[(\boldsymbol{v}_h, q_h); (\boldsymbol{u}_h, q_h)] + \boldsymbol{c}(\boldsymbol{w}_h; \boldsymbol{v}_h, \boldsymbol{u}_h)}{\|(\boldsymbol{v}_h, q_h)\|},\end{aligned}$$

from which,

$$\begin{aligned}\sup_{\mathbf{0}\neq(\boldsymbol{v}_h,q_h)\in\mathrm{V}_h\times\Pi_h} \mathcal{A}_{\boldsymbol{w}_h}[(\boldsymbol{v}_h, q_h); (\boldsymbol{u}_h, q_h)] &\geq \sup_{\mathbf{0}\neq(\boldsymbol{v}_h,q_h)\in\mathrm{V}_h\times\Pi_h} \frac{|\mathcal{C}_h[(\boldsymbol{v}_h, q_h); (\boldsymbol{u}_h, p_h)] + \boldsymbol{c}(\boldsymbol{w}_h; \boldsymbol{v}_h, \boldsymbol{u}_h)|}{\|(\boldsymbol{v}_h, q_h)\|} \\ &\geq \sup_{\mathbf{0}\neq(\boldsymbol{v}_h,q_h)\in\mathrm{V}_h\times\Pi_h} \frac{|\mathcal{C}_h[(\boldsymbol{v}_h, q_h); (\boldsymbol{u}_h, p_h)]|}{\|(\boldsymbol{v}_h, q_h)\|} - \frac{|\boldsymbol{c}(\boldsymbol{w}_h; \boldsymbol{v}_h, \boldsymbol{u}_h)|}{\|(\boldsymbol{v}_h, q_h)\|},\end{aligned}$$

for all $\mathbf{0} \neq (\boldsymbol{v}_h, q_h) \in \mathrm{V}_h \times \Pi_h$, which together with Theorem 3, implies

$$\sup_{\mathbf{0}\neq(\boldsymbol{v}_h,q_h)\in \mathrm{V}_h\times\Pi_h} \mathcal{A}_{\boldsymbol{w}_h}[(\boldsymbol{v}_h, q_h); (\boldsymbol{u}_h, p_h)] \geq \sup_{\mathbf{0}\neq(\boldsymbol{v}_h,q_h)\in \mathrm{V}_h\times\Pi_h} \frac{\mathcal{C}_h[(\boldsymbol{v}_h, q_h); (\boldsymbol{u}_h, p_h)]}{\|(\boldsymbol{v}_h, q_h)\|} - \|\boldsymbol{w}_h\|_{1,h}\|(\boldsymbol{u}_h, p_h)\|. \quad (40)$$

Therefore, using the fact that $\mathcal{C}_h[\cdot;\cdot]$ is symmetric, from the inequality in Theorem 4 and (40) we obtain

$$\sup_{\mathbf{0}\neq(\boldsymbol{v}_h,q_h)\in \mathrm{V}_h\times\Pi_h} \mathcal{A}_{\boldsymbol{w}_h}[(\boldsymbol{v}_h, q_h); (\boldsymbol{u}_h, p_h)] \geq \hat{\alpha}\|(\boldsymbol{u}_h, p_h)\| - \|\boldsymbol{w}_h\|_{1,h}\|(\boldsymbol{u}_h, p_h)\|,$$

which combined with (38), yields

$$\sup_{\mathbf{0}\neq(\boldsymbol{v}_h,q_h)\in \mathrm{V}_h\times\Pi_h} \mathcal{A}_{\boldsymbol{w}_h}[(\boldsymbol{v}_h, q_h); (\boldsymbol{u}_h, p_h)] \geq \frac{\hat{\alpha}}{2}\|(\boldsymbol{u}_h, p_h)\| > 0 \quad \forall(\boldsymbol{u}_h, p_h) \in \mathrm{V}_h \times \Pi_h, (\boldsymbol{u}_h, p_h) \neq 0. \quad (41)$$

By examining (39) and (41), we can deduce that $\mathcal{A}_{\boldsymbol{w}_h}(\cdot,\cdot)$ satisfies the conditions of the Banach Nečas Babuška theorem ([26], Theorem 2.6). This guarantees the existence of a unique solution $(\boldsymbol{u}_h, p_h) \in \mathrm{V}_h \times \Pi_h$ to (24), or equivalently, the existence of a unique $\boldsymbol{u}_h \in \mathrm{V}_h$ such that $\mathcal{J}_h(\boldsymbol{w}_h) = \boldsymbol{u}_h$. Furthermore, from (39) and (36) we derive the following inequality:

$$\|\boldsymbol{u}_h\|_{1,h} \leq \|(\boldsymbol{u}_h, p_h)\| \leq \frac{1}{\hat{\alpha}}\|\boldsymbol{f}\|_{\mathrm{V}'}.$$

This concludes the proof by showing that $\boldsymbol{u_h} \in \boldsymbol{K_h}$. □

3.1.3. Well-posedness of the discrete problem

The subsequent theorem establishes the well-posedness of Nitsche's scheme (24).

Theorem 6. *Let $\boldsymbol{f} \in \mathrm{V}'$ such that*

$$\frac{2}{\hat{\alpha}^2}\|\boldsymbol{f}\|_{\mathrm{V}'} \leq 1. \quad (42)$$

Then, there exists a unique $(\boldsymbol{u}_h, p_h) \in \mathrm{V}_h \times \Pi_h$ solution to (23). In addition, there exists $C = \max\{\frac{1}{\hat{\alpha}}, \frac{2}{\hat{\alpha}}\} > 0$, independent of h, such that

$$\|\boldsymbol{u}_h\|_{1,h} + \|p_h\|_{0,\Omega} \leq C\|\boldsymbol{f}\|_{\mathrm{V}'}. \quad (43)$$

Proof. According to the relations given in (32), we aim to establish the well-posedness of (23). This can be accomplished by using Banach's theorem to demonstrate that $\mathcal{J}_h$ possesses a unique fixed point in $\boldsymbol{K}_h$.

The validity of Assumption (42) as shown in Theorem 5, ensures that $\mathcal{J}_h$ is well-defined. Now, let $\boldsymbol{w}_{h1}$, $\boldsymbol{w}_{h2}$, $\boldsymbol{u}_{h1}$, $\boldsymbol{u}_{h2} \in \boldsymbol{K}_h$, be such that $\boldsymbol{u}_{h1} = \mathcal{J}_h(\boldsymbol{w}_{h1})$ and $\boldsymbol{u}_{h2} = \mathcal{J}_h(\boldsymbol{w}_{h2})$. By employing the definition of $\mathcal{J}_h$ and (36), it follows that there exist unique $p_{h1}, p_{h2} \in L^2(\Omega)$, satisfies the following equations:

$$\mathcal{A}_{\boldsymbol{w}_{h1}}[(\boldsymbol{u}_{h1}, p_{h1}); (\boldsymbol{v}_h, q_h)] = \mathcal{F}(\boldsymbol{v}_h), \quad \text{and} \quad \mathcal{A}_{\boldsymbol{w}_{h2}}[(\boldsymbol{u}_{h2}, p_{h2}); (\boldsymbol{v}_h, q_h)] = \mathcal{F}(\boldsymbol{v}_h) \quad \forall(\boldsymbol{v}_h, q_h) \in \mathrm{V}_h \times \Pi_h.$$

By adding and subtracting appropriate terms, we can derive the following:

$$\mathcal{A}_{\boldsymbol{w}_{h1}}[(\boldsymbol{u}_{h1} - \boldsymbol{u}_{h2}; p_{h1} - p_{h2}), (\boldsymbol{v}_h, q_h)] = -\boldsymbol{c}(\boldsymbol{w}_{h1} - \boldsymbol{w}_{h2}; \boldsymbol{u}_{h2}, \boldsymbol{v}_h) \quad \forall(\boldsymbol{v}_h, q_h) \in \mathrm{V}_h \times \Pi_h. \quad (44)$$

Given that $\boldsymbol{w}_{h1} \in \boldsymbol{K}_h$ and using (44), (39), and Theorem 3, we can deduce:

$$\begin{aligned}
\frac{\hat{\alpha}}{2}\|\boldsymbol{u}_{h1} - \boldsymbol{u}_{h2}\|_1 &\leq \sup_{\mathbf{0}\neq(\boldsymbol{v}_h,p_h)\in \mathrm{V}_h\times\Pi_h} \frac{\mathcal{A}_{\boldsymbol{w}_{h1}}[(\boldsymbol{u}_{h1} - \boldsymbol{u}_{h2}, p_{h1} - p_{h2}); (\boldsymbol{v}_h, q_h)]}{\|(\boldsymbol{v}_h, q_h)\|} \\
&= \sup_{\mathbf{0}\neq(\boldsymbol{v}_h,q_h)\in \mathrm{V}_h\times\Pi_h} \frac{-\boldsymbol{c}(\boldsymbol{w}_{h1} - \boldsymbol{w}_{h2}; \boldsymbol{u}_{h2}, \boldsymbol{v}_h)}{\|(\boldsymbol{v}_h, q_h)\|} \\
&\leq \|\boldsymbol{w}_{h1} - \boldsymbol{w}_{h2}\|_{1,h}\|\boldsymbol{u}_{h2}\|_{1,h},
\end{aligned}$$

which together with the fact that $\boldsymbol{u}_{h2} \in \boldsymbol{K}_h$, implies

$$\|\boldsymbol{u}_{h1} - \boldsymbol{u}_{h2}\|_{1,h} \leq \frac{1}{\hat{\alpha}}\|\boldsymbol{f}\|_{\mathrm{V}'}\|\boldsymbol{w}_{h1} - \boldsymbol{w}_{h2}\|_{1,h}$$

$$\|\boldsymbol{u}_{h1} - \boldsymbol{u}_{h2}\|_{1,h} \leq \frac{\hat{\alpha}}{2}\|\boldsymbol{w}_{h1} - \boldsymbol{w}_{h2}\|_{1,h}.$$

Assumption (42) directly implies that $\mathcal{J}_h$ is a contraction mapping. Now, to establish the estimate (43), let $\boldsymbol{u}_h \in \boldsymbol{K}_h$ be the unique fixed point of $\mathcal{J}_h$ and let $\boldsymbol{u}_h \in \mathrm{V}_h$ be the unique solution of (23) with $(\boldsymbol{u}_h, p_h) \in \mathrm{V}_h \times \Pi_h$. By the definition of $\boldsymbol{K}_h$, it is evident that $\boldsymbol{u}_h$ satisfies the following

$$\|\boldsymbol{u}_h\|_{1,h} \leq \hat{\alpha}^{-1}\|\boldsymbol{f}\|_{\mathrm{V}'}.$$

Consequently, utilizing (39) on $\mathcal{A}_{\boldsymbol{u}_h}$, referring back to the definition of $\mathcal{A}_{\boldsymbol{u}_h}$ given in (35), and using the fact that $(\boldsymbol{u}_h, p_h)$ satisfies (23), we obtain

$$\|p_h\|_{0,\Omega} \leq \|(\boldsymbol{u}_h, p_h)\| \leq \frac{2}{\hat{\alpha}} \sup_{\mathbf{0}\neq(\boldsymbol{v}_h,q_h)\in \mathrm{V}_h\times\Pi_h} \frac{\mathcal{A}_{\boldsymbol{u}_h}[(\boldsymbol{u}_h, p_h); (\boldsymbol{v}_h, q_h)]}{\|(\boldsymbol{v}_h, q_h)\|} = \frac{2}{\hat{\alpha}} \sup_{\mathbf{0}\neq(\boldsymbol{v}_h,q_h)\in \mathrm{V}_h\times\Pi_h} \frac{\mathcal{F}(\boldsymbol{v}_h)}{\|(\boldsymbol{v}_h, p_h)\|},$$

Thus

$$\|p_h\|_{0,\Omega} \leq \frac{2}{\hat{\alpha}}\|\boldsymbol{f}\|_{\mathrm{V}'}.$$

□

Let us denote I_h be the interpolation operator. Under usual assumptions, the following approximation property hold.

Lemma 10. *Let there exists $C_9 > 0$ and $C_{10} > 0$, independent of h, such that for each $\boldsymbol{u} \in \boldsymbol{H}^{l+1}(K)$ with $0 \leq l \leq k$, there holds*

$$\|\boldsymbol{u} - \mathrm{I}_h(\boldsymbol{u})\|_{\boldsymbol{L}^2(K)} \leq C_9 \frac{h_K^{l+2}}{\rho_K}|\boldsymbol{u}|_{\boldsymbol{H}^{l+1}(K)} \leq \hat{C}_1 h_K^{l+1}|\boldsymbol{u}|_{\boldsymbol{H}^{l+1}(K)}$$
$$|\boldsymbol{u} - \mathrm{I}_h(\boldsymbol{u})|_{\boldsymbol{H}^1(K)} \leq C_{10} \frac{h_K^{l+2}}{\rho_K^2}|\boldsymbol{u}|_{\boldsymbol{H}^{l+1}(K)} \leq \hat{C}_2 h_K^{l}|\boldsymbol{u}|_{\boldsymbol{H}^{l+1}(K)}$$

where h_K is the diameter of K, ρ_K is the diameter of the largest sphere contained in K, and k is the degree of the polynomial. The constants $\hat{C}_1$ and $\hat{C}_2$ are defined as

$$\hat{C}_1 = C_9 \frac{h_K}{\rho_K} \leq C_9\hat{\sigma} \text{ and } \hat{C}_2 = C_{10}\frac{h_K^2}{\rho_K^2} \leq C_{10}\hat{\sigma}^2,$$

Here $\hat{\sigma}$ denotes the shape regularity constant.

Proof. See [11]. □

4. *A priori* ERROR BOUNDS

This section aims to establish the convergence of Nitsche's scheme (23) and determine the convergence rate. We derive the corresponding Cèa's estimate.

Theorem 7. *Assume that*

$$\frac{2}{\alpha\hat{\alpha}}\|\boldsymbol{f}\|_{\mathrm{V}'} \leq \frac{1}{2}, \tag{45}$$

with α and $\hat{\alpha}$ being the positive constants in (18) *and Theorem 4, respectively. Let $(\boldsymbol{u}, p) \in \mathrm{V} \times \Pi$ and $(\boldsymbol{u}_h, p_h) \in \mathrm{V}_h \times \Pi_h$ be the unique solutions of problems* (7) *and* (23)*, respectively. Then there exists $C_{cea}(\nu, \beta, \Omega) = (1+\frac{2}{\hat{\alpha}}) > 0$, independent of h, such that*

$$\|(\boldsymbol{u} - \boldsymbol{u}_h, p - p_h)\| \leq C_{cea} \inf_{\boldsymbol{0}\neq(\boldsymbol{v}_h,q_h)\in \mathrm{V}_h\times\Pi_h} \|(\boldsymbol{u} - \boldsymbol{v}_h, p - q_h)\|. \tag{46}$$

Proof. In order to simplify the subsequent analysis, we define $\boldsymbol{e}_{\mathrm{u}} = \boldsymbol{u} - \boldsymbol{u}_h$ and $\boldsymbol{e}_p = p - p_h$, and for any $(\boldsymbol{z}_h, \zeta_h) \in \mathrm{V}_h \times \Pi_h$, we write

$$\boldsymbol{e}_{\boldsymbol{u}} = \xi_{\boldsymbol{u}} + \chi_{\boldsymbol{u}} = (\boldsymbol{u} - \boldsymbol{z}_h) + (\boldsymbol{z}_h - \boldsymbol{u}_h), \quad \text{and} \quad \boldsymbol{e}_p = \xi_p + \chi_p = (p - \zeta_h) + (\zeta_h - p_h). \tag{47}$$

By recalling the definition of the bilinear forms $\mathcal{C}$ and $\mathcal{C}_h$ in (16) and (33), respectively, and considering (7) and (23), we can observe the validity of following identities

$$\mathcal{C}_h[(\boldsymbol{u}, p); (\boldsymbol{v}, q)] + \boldsymbol{c}(\boldsymbol{u}; \boldsymbol{u}, \boldsymbol{v}) = \mathcal{F}(\boldsymbol{v}) \quad \forall(\boldsymbol{v}, q) \in \mathrm{V} \times \Pi.$$

and

$$\mathcal{C}_h[(\boldsymbol{u}_h, p_h); (\boldsymbol{v}_h, q_h)] + \boldsymbol{c}(\boldsymbol{u}_h; \boldsymbol{u}_h, \boldsymbol{v}_h) = \mathcal{F}(\boldsymbol{v}_h) \quad \forall(\boldsymbol{v}_h, q_h) \in \mathrm{V}_h \times \Pi_h.$$

Based on these observations, we can deduce the Galerkin orthogonality property

$$\mathcal{C}_h[(\boldsymbol{e}_{\boldsymbol{u}}, \boldsymbol{e}_p); (\boldsymbol{v}_h, q_h)] + [\boldsymbol{c}(\boldsymbol{u}; \boldsymbol{u}, \boldsymbol{v}_h) - \boldsymbol{c}(\boldsymbol{u}_h; \boldsymbol{u}_h, \boldsymbol{v}_h)] = 0, \quad \forall(\boldsymbol{v}_h, q_h) \in \mathrm{V}_h \times \Pi_h. \tag{48}$$

Subsequently, by utilizing the decompositions given in (47), the definition of $\mathcal{A}_{\mathrm{w}}$ in (35) for discrete $\mathcal{A}_{\mathrm{w}_h}$, and the identity

$$\boldsymbol{c}(\boldsymbol{u}; \boldsymbol{u}, \boldsymbol{v}_h) = \boldsymbol{c}(\boldsymbol{u} - \boldsymbol{u}_h; \boldsymbol{u}, \boldsymbol{v}_h) + \boldsymbol{c}(\boldsymbol{u}_h; \boldsymbol{u}, \boldsymbol{v}_h). \tag{49}$$

Now, using (35), (49), and (48), we deduce that for all $(\boldsymbol{v}_h, q_h) \in \mathrm{V}_h \times \Pi_h$, the following relationship holds

$$\begin{aligned}
\mathcal{A}_{\boldsymbol{u}_{\mathrm{h}}}[(\chi_{\boldsymbol{u}}, \chi_p); (\boldsymbol{v}_h, q_h)] &= \mathcal{C}_h[(\chi_{\boldsymbol{u}}, \chi_p), (\boldsymbol{v}_h, q_h)] + \boldsymbol{c}(\boldsymbol{u}_h; \chi_{\boldsymbol{u}}, \boldsymbol{v}_h)\\
&= -\mathcal{C}_h[(\xi_{\boldsymbol{u}}, \xi_p); (\boldsymbol{v}_h, q_h)] + \mathcal{C}_h[(\boldsymbol{e}_{\boldsymbol{u}}, \boldsymbol{e}_p); (\boldsymbol{v}_h, q_h)] + \boldsymbol{c}(\boldsymbol{u}_h; \chi_{\boldsymbol{u}}, \boldsymbol{v}_h)\\
&= -\mathcal{C}_h[(\xi_{\boldsymbol{u}}, \xi_p); (\boldsymbol{v}_h, q_h)] - \boldsymbol{c}(\boldsymbol{u} - \boldsymbol{u}_h; \boldsymbol{u}, \boldsymbol{v}_h) - \boldsymbol{c}(\boldsymbol{u}_h; \boldsymbol{u}, \boldsymbol{v}_h)\\
&\quad + \boldsymbol{c}(\boldsymbol{u}_h; \boldsymbol{u}_h, \boldsymbol{v}_h) + \boldsymbol{c}(\boldsymbol{u}_h; \chi_{\boldsymbol{u}}, \boldsymbol{v}_h)\\
&= -\mathcal{C}_h[(\xi_{\boldsymbol{u}}, \xi_p); (\boldsymbol{v}_h, q_h)] - \boldsymbol{c}(\xi_{\boldsymbol{u}} + \chi_{\boldsymbol{u}}; \boldsymbol{u}, \boldsymbol{v}_h) - \boldsymbol{c}(\boldsymbol{u}_h; \xi_{\boldsymbol{u}} + \chi_{\boldsymbol{u}}, \boldsymbol{v}_h) + \boldsymbol{c}(\boldsymbol{u}_h; \chi_{\boldsymbol{u}}, \boldsymbol{v}_h)\\
&= -\mathcal{C}_h[(\xi_{\boldsymbol{u}}, \xi_p); (\boldsymbol{v}_h, q_h)] - \boldsymbol{c}(\xi_{\boldsymbol{u}}; \boldsymbol{u}, \boldsymbol{v}_h) - \boldsymbol{c}(\chi_{\boldsymbol{u}}; \boldsymbol{u}, \boldsymbol{v}_h) - \boldsymbol{c}(\boldsymbol{u}_h; \xi_{\boldsymbol{u}}, \boldsymbol{v}_h).
\end{aligned}$$

which together with the definition of $\mathcal{C}_h$ given in equation (33), implies

$$\begin{aligned}
\mathcal{A}_{\boldsymbol{u}_{\mathrm{h}}}[(\chi_{\boldsymbol{u}}, \chi_p); (\boldsymbol{v}_h, q_h)] = &-\boldsymbol{A}_h(\xi_{\boldsymbol{u}}, \boldsymbol{v}_h) - \boldsymbol{B}_h(\xi_{\boldsymbol{u}}, q_h) - \boldsymbol{B}_h(\boldsymbol{v}_h, \xi_p) - \boldsymbol{c}(\xi_{\boldsymbol{u}}; \boldsymbol{u}, \boldsymbol{v}_h)\\
&- \boldsymbol{c}(\chi_{\boldsymbol{u}}; \boldsymbol{u}, \boldsymbol{v}_h) - \boldsymbol{c}(\boldsymbol{u}_h; \xi_{\boldsymbol{u}}, \boldsymbol{v}_h),
\end{aligned} \tag{50}$$

for all $(\boldsymbol{v}_h, q_h) \in \mathrm{V}_h \times \Pi_h$. Next, utilizing the discrete inf-sup condition (41) at the left hand side of (50), and applying the continuity properties of $\boldsymbol{A}, \boldsymbol{B}$, and $\boldsymbol{c}$ stated in Theorem 3 to the right hand side of (50), we can derive the following

$$\|\chi_{\boldsymbol{u}}\|_{1,h} + \|\chi_p\|_0 \lesssim \frac{2}{\hat{\alpha}\|(\boldsymbol{v}_h, q_h)\|}\big(\|\xi_{\boldsymbol{u}}\|_{1,h}\|\boldsymbol{v}_h\|_{1,h} + \|\xi_{\boldsymbol{u}}\|_{1,h}\|q_h\|_0 + \|\xi_{\boldsymbol{p}}\|_0\|\boldsymbol{v}_h\|_{1,h} + \|\xi_{\boldsymbol{u}}\|_{1,h}\|\boldsymbol{v}_h\|_{1,h}\|\boldsymbol{u}\|_1$$

$$
\begin{aligned}
&+ \|\chi_{\boldsymbol{u}}\|_{1,h}\|\boldsymbol{v}_h\|_{1,h}\|\boldsymbol{u}\|_1 + \|\xi_{\boldsymbol{u}}\|_{1,h}\|\boldsymbol{v}_h\|_{1,h}\|\boldsymbol{u}_h\|_{1,h}\big)\\
&\lesssim \frac{2}{\hat{\alpha}}\big(\|\xi_p\|_0 + (2 + \|\boldsymbol{u}_h\|_{1,h} + \|\boldsymbol{u}\|_1)\|\xi_{\boldsymbol{u}}\|_{1,h} + \|\chi_{\boldsymbol{u}}\|_{1,h}\|\boldsymbol{u}\|_1\big)\\
&\lesssim \frac{2}{\hat{\alpha}}\big(\|\xi_p\|_0 + (2 + \|\boldsymbol{u}_h\|_{1,h} + \|\boldsymbol{u}\|_1)\|\xi_{\boldsymbol{u}}\|_{1,h} + \|\chi_{\boldsymbol{u}}\|_{1,h}\|\boldsymbol{u}\|_1\big).
\end{aligned}
$$

$$
\|\chi_p\|_0 + \left(1 - \frac{2}{\hat{\alpha}}\|\boldsymbol{u}\|_1\right)\|\chi_{\boldsymbol{u}}\|_{1,h} \lesssim \frac{2}{\hat{\alpha}}\big(\|\xi_p\|_0 + \{2 + \|\boldsymbol{u}_h\|_{1,h} + \|\boldsymbol{u}\|_1\}\|\xi_{\boldsymbol{u}}\|_{1,h}\big). \tag{51}
$$

Therefore, by taking into account the fact that $\boldsymbol{u} \in \boldsymbol{K}$ and $\boldsymbol{u}_h \in \boldsymbol{K}_h$ based respectively on assumptions (45) and (51), we can conclude that

$$
\|\chi_p\|_0 + \|\chi_{\boldsymbol{u}}\|_{1,h} \lesssim \big(\|\xi_p\|_0 + \|\xi_{\boldsymbol{u}}\|_{1,h}\big). \tag{52}
$$

In this way, from (47), (52) and the triangle inequality we obtain

$$
\|(\boldsymbol{e}_p, \boldsymbol{e}_{\boldsymbol{u}})\| \le \|(\chi_p, \chi_{\boldsymbol{u}})\| + \|(\xi_p, \xi_{\boldsymbol{u}})\| \lesssim \|(\xi_p, \xi_{\mathrm{u}})\|.
$$

This, together with the fact that $(\boldsymbol{z}_h, \zeta_h) \in \mathrm{V}_h \times \Pi_h$ is arbitrary, leads to the conclusion of the proof. ☐

Theorem 8. *Let $(\boldsymbol{u}, p) \in \mathrm{V} \times \Pi$ and $(\boldsymbol{u}_h, p_h) \in \mathrm{V}_h \times \Pi_h$ denotes the unique solutions of the continuous problem (7) and discrete problem (23), respectively, with $\boldsymbol{f}$ satisfying (45). Suppose that $(\boldsymbol{u}, p) \in (\boldsymbol{H}^{l+1}(\Omega) \cap \mathrm{V}) \times (H^l(\Omega) \cap \Pi)$ with $l \ge 1$, Then there exists $C_{rate}\,(\nu, \beta, \Omega) = (1 + \frac{2}{\hat{\alpha}}) \max\{\hat{C}_1, \hat{C}_2\} > 0$, independent of h, such that*

$$
\|(\boldsymbol{u} - \boldsymbol{u}_h, p - p_h)\| \le C_{rate}\, h^l \big\{|\boldsymbol{u}|_{\boldsymbol{H}^{l+1}(\Omega)} + |p|_{H^l(\Omega)}\big\}.
$$

Proof. The conclusion can be easily obtained by directly applying Theorem 7 and Lemma 10. ☐

5. Stabilized formulation for high Reynolds numbers

The complex dynamics described by the Navier–Stokes equations at high Reynolds numbers lead to numerical instabilities, presenting significant challenges for their accurate numerical approximation, particularly affecting the accuracy of the finite element method. This section provides a VMS-LES formulation with Nitsche for the Navier–Stokes equations with slip boundary conditions. In Section 6 we show numerical evidence of the utility of the VMS-LES method within a Nitsche framework in solving the Navier–Stokes equations for high Reynolds number flows. In a time interval $(0, T]$ with $T > 0$, the model problem is formulated as follows:

$$
\begin{aligned}
\partial_t \boldsymbol{u} - \nu\Delta\boldsymbol{u} + (\boldsymbol{u}\cdot\nabla)\boldsymbol{u} + \nabla p &= \boldsymbol{f} \quad \text{in}\, \Omega \times (0, T),\\
\operatorname{div} \boldsymbol{u} &= 0 \quad \text{in}\, \Omega \times (0, T),\\
\boldsymbol{u} &= \boldsymbol{0} \quad \text{on}\, \Gamma_D \times (0, T),\\
\boldsymbol{u}\cdot\boldsymbol{n} &= 0 \quad \text{on}\, \Gamma_{\text{Nav}} \times (0, T),\\
\nu\boldsymbol{n}^t D(\boldsymbol{u})\boldsymbol{\tau}^i + \beta\boldsymbol{u}\cdot\boldsymbol{\tau}^i &= 0 \quad \text{on}\, \Gamma_{\text{Nav}} \times (0, T), \quad i = 1\ldots(d-1),\\
\boldsymbol{u}(\boldsymbol{0}) &= \boldsymbol{0} \quad \text{in}\, \Omega \times \{0\},\\
(p, 1)_\Omega &= 0.
\end{aligned} \tag{53}
$$

The weak formulation of problem (53) can be written as: for all $t \in (0, T]$, find $(\boldsymbol{u}, p) \in \mathcal{Y}_0 = \mathrm{V} \times \Pi$ with $\boldsymbol{u}(0) = 0$ such that

$$
\mathcal{A}[(\boldsymbol{u}, p); (\boldsymbol{v}, q)] = \mathcal{F}(\boldsymbol{v}) \quad \forall (\boldsymbol{v}, q)\mathrm{V} \times \Pi, \tag{54}
$$

where

$$\mathcal{A}[(\boldsymbol{u},p);(\boldsymbol{v},q)] \coloneqq (\partial_t \boldsymbol{u},\boldsymbol{v})_\Omega + \frac{\nu}{2}(D(\boldsymbol{u}),D(\boldsymbol{v}))_\Omega + (\boldsymbol{u}\cdot\nabla\boldsymbol{u},\boldsymbol{v})_\Omega - (p,\nabla\cdot\boldsymbol{v})_\Omega - (q,\nabla\cdot\boldsymbol{u})_\Omega$$
$$+ \int_{\Gamma_{\mathrm{Nav}}} \beta \sum_i^{d-1} \big(\boldsymbol{\tau}^i\cdot\boldsymbol{v}\big)\big(\boldsymbol{\tau}^i\cdot\boldsymbol{u}\big)\,\mathrm{d}s,$$
$$\mathcal{F}(\boldsymbol{v}) \coloneqq \langle \boldsymbol{f},\boldsymbol{v}\rangle_\Omega.$$

5.1. The VMS-LES formulation

The VMS technique involves decomposing the solution into coarser and finer scales. As a result, we decompose the weak formulation of the Navier–Stokes equations (54) into two subproblems, considering the coarse scale and the fine scale. The finite element method approximates the coarse-scale solution, while the fine-scale solution is formulated analytically. Now, we decompose the space into the direct sum of two subspaces:

$$\mathcal{Y}_0 = \mathcal{V}_0^h \oplus \mathcal{V}_0' \tag{55}$$

where $\mathcal{V}_0^h$ known as coarse scale spaces, are the finite element spaces used for the numerical discretization, *i.e.*,

$$\mathcal{V}_0^h = \mathrm{V}_h \times \Pi_h,$$

and $\mathcal{V}_0'$ are infinite dimensional, known as the fine scale spaces, and orthogonal to $\mathcal{V}_0^h$ respectively. Then, we have the following decompositions from (55):

$$\boldsymbol{u} = \boldsymbol{u}_h + \boldsymbol{u}',$$
$$p = p_h + p',$$

where $(\boldsymbol{u},p)\in\mathcal{Y}_0$ and this is the starting point of VMS-LES method *i.e.*, the separation of the flow field into resolved scales $(\boldsymbol{u}_h,p_h)$ and unresolved scales $(\boldsymbol{u}',p')$. Following the approach proposed in [3], Performing the two-scale decomposition on the problem (54), we obtain two subproblems, one for the coarse and other for the fine scales:

$$\mathcal{A}\big[\boldsymbol{V}_h;\boldsymbol{U}_h+\boldsymbol{U}'\big] = \mathcal{F}(\boldsymbol{V}_h) \tag{56}$$

$$\mathcal{A}\big[\boldsymbol{V}';\boldsymbol{U}_h+\boldsymbol{U}'\big] = \mathcal{F}(\boldsymbol{V}') \tag{57}$$

where the abbreviations $\boldsymbol{U}=(\boldsymbol{u},p)$ and $\boldsymbol{V}=(\boldsymbol{v},q)$ are used for simplicity. The fine-scale solution is typically modeled analytically, expressed in terms of both the problems data and the coarse-scale solution, and then substituted into the coarse-scale subproblem. A finite-dimensional system for the coarse-scale solution is obtained by projecting the fine-scale solution into the coarse-scale solution.

The solution of (57) is represented as

$$\boldsymbol{U}' = F_{\boldsymbol{U}}(\boldsymbol{R}(\boldsymbol{U}_h)), \tag{58}$$

which can be interpreted as the unresolved scales derived as a function of the residual of the resolved scales. By substituting (58) into the resolved scales equation (56), a unified set of equations for the resolved scales is obtained.

The objective is to approximate $F_{\boldsymbol{U}}$ using models that are not dependent on the underlying physics of high Reynolds number flows but are derived solely based on mathematical reasoning. Finally, we adopt a similar approach to [19] in modeling the fine-scale velocity and pressure variables as:

$$\boldsymbol{u}' \simeq -\mathcal{S}_M(\boldsymbol{u}_h)\boldsymbol{r}_M(\boldsymbol{u}_h,p_h)$$
$$p' \simeq -\mathcal{S}_C(\boldsymbol{u}_h)r_C(\boldsymbol{u}_h)$$

where $\boldsymbol{r}_M(\boldsymbol{u}_h, p_h)$ and $r_C(\boldsymbol{u}_h)$ indicate the strong residuals of the momentum and continuity equations:

$$\begin{aligned}
&\boldsymbol{r}_M(\boldsymbol{u}_h, p_h) = \partial_t \boldsymbol{u}_h + \boldsymbol{u}_h \cdot \nabla \boldsymbol{u}_h + \nabla p_h - \nu \Delta \boldsymbol{u}_h - \boldsymbol{f},\\
&r_C(\boldsymbol{u}_h) = \nabla \cdot \boldsymbol{u}_h,
\end{aligned}$$

respectively. Moreover, $\mathcal{S}_M$ and $\mathcal{S}_C$ are the stabilization parameters designed by a specific Fourier analysis applied in the framework of stabilized methods, which we choose similarly to [9] as:

$$\begin{aligned}
&\mathcal{S}_M(\boldsymbol{u}_h) = \left(\frac{\sigma^2}{(\Delta t)^2} + \boldsymbol{u}_h \cdot \boldsymbol{G} \boldsymbol{u}_h + C_r \nu^2 \boldsymbol{G} : \boldsymbol{G}\right)^{-1/2}\\
&\mathcal{S}_C(\boldsymbol{u}_h) = (\mathcal{S}_M(\boldsymbol{u}_h) \boldsymbol{g} \cdot \boldsymbol{g})^{-1}
\end{aligned} \tag{59}$$

where Δt denotes the time step, while σ represents the order of the BDF (Backward Differentiation Formulas) time scheme [52]. Furthermore, the constant $C_k = 60 \cdot 2^{k-2}$ is calculated using an inverse inequality which depends on the polynomial degree k associated with the velocity finite element space [27]. Moreover, $\boldsymbol{G}$ and $\boldsymbol{g}$ correspond to the metric tensor and vector, respectively defined as

$$\begin{aligned}
&G_{ij} = \sum_{k=1}^{d} \frac{\partial \xi_k}{\partial x_i} \frac{\partial \xi_k}{\partial x_j},\\
&g_i = \sum_{k=1}^{d} \frac{\partial \xi_k}{\partial x_i},
\end{aligned}$$

with $\boldsymbol{x} = \{x_i\}_{i=1}^d$ represents the coordinates of element K in physical space, $\boldsymbol{\xi} = \{\xi_i\}_{i=1}^d$ represents the coordinates of element $\hat{K}$ in parametric space, and $\frac{\partial \boldsymbol{\xi}}{\partial \boldsymbol{x}}$ represents the inverse Jacobian of the element mapping between the reference and physical domains. We make the same assumptions as [9]:

$$\left\{\begin{array}{l}
\frac{\partial \boldsymbol{v}_h}{\partial t} = \boldsymbol{0},\\
\boldsymbol{u}' = \boldsymbol{0} \,\text{on}\, \Gamma,\\
(D(\boldsymbol{v}_h), D(\boldsymbol{u}'))_\Omega = 0.
\end{array}\right. \tag{60}$$

By explicitly expressing the left-hand side of (56) and adding the Nitsche terms to the action of the Laplace distribution, we arrive at the following result:

$$\begin{aligned}
\mathcal{A}[\boldsymbol{V}_h; \boldsymbol{U}_h + \boldsymbol{U}'] = {}& (\partial_t \boldsymbol{u}_h, \boldsymbol{v}_h)_\Omega + (\partial_t \boldsymbol{u}', \boldsymbol{v}_h)_\Omega + \frac{\nu}{2}(D(\boldsymbol{u}_h), D(\boldsymbol{v}_h))_\Omega + \frac{\nu}{2}(D(\boldsymbol{u}'), D(\boldsymbol{v}_h))_\Omega\\
&+ ((\boldsymbol{u}_h + \boldsymbol{u}') \cdot \nabla(\boldsymbol{u}_h + \boldsymbol{u}'), \boldsymbol{v}_h)_\Omega - (p_h + p', \nabla \cdot \boldsymbol{v}_h)_\Omega - (q_h, \nabla \cdot (\boldsymbol{u}_h + \boldsymbol{u}'))_\Omega\\
&+ \sum_{E \in \mathcal{E}_{\text{Nav}}} \Bigg(- \int_E \boldsymbol{n}^t (\nu D(\boldsymbol{u}_h + \boldsymbol{u}') - (p_h + p') I) \boldsymbol{n} (\boldsymbol{n} \cdot \boldsymbol{v}_h) \,\mathrm{d}s\\
&- \int_E \boldsymbol{n}^t (\nu D(\boldsymbol{v}_h) - q_h I) \boldsymbol{n} (\boldsymbol{n} \cdot (\boldsymbol{u}_h + \boldsymbol{u}')) \,\mathrm{d}s + \int_E \beta \sum_i^{d-1} \big(\boldsymbol{\tau}^i \cdot \boldsymbol{v}_h\big)\big(\boldsymbol{\tau}^i \cdot (\boldsymbol{u}_h + \boldsymbol{u}')\big) \,\mathrm{d}s\\
&+ \gamma \int_E {h_e}^{-1} ((\boldsymbol{u}_h + \boldsymbol{u}') \cdot \boldsymbol{n})(\boldsymbol{v}_h \cdot \boldsymbol{n}) \,\mathrm{d}s \Bigg)
\end{aligned}$$

Thereafter, we apply integration by parts to the fine-scale terms that appear in the coarse-scale equations, by considering the aforementioned assumption (60) and we get

$$\begin{aligned}
&\mathcal{A}[\boldsymbol{V}_h;\boldsymbol{U}_h+\boldsymbol{U}'] \\
&\quad= \sum_{K\in\mathcal{K}_h}\Big((\partial_t \boldsymbol{u}_h,\boldsymbol{v}_h)_K + \frac{\nu}{2}(D(\boldsymbol{u}_h),D(\boldsymbol{v}_h))_K + (\boldsymbol{u}_h\cdot\nabla\boldsymbol{u}_h,\boldsymbol{v}_h)_K - (p_h,\nabla\cdot\boldsymbol{v}_h)_K - (q_h,\nabla\cdot\boldsymbol{u}_h)_K\Big) \\
&\qquad+ \sum_{E\in\mathcal{E}_{\mathrm{Nav}}}\Big(-\int_E \boldsymbol{n}^t(\nu D(\boldsymbol{u}_h)-p_h I)\boldsymbol{n}(\boldsymbol{n}\cdot\boldsymbol{v}_h)\,\mathrm{d}s - \int_E \boldsymbol{n}^t(\nu D(\boldsymbol{v}_h)-q_h I)\boldsymbol{n}(\boldsymbol{n}\cdot\boldsymbol{u}_h)\,\mathrm{d}s \\
&\qquad+ \int_E \beta\sum_i^{d-1}(\boldsymbol{\tau}^i\cdot\boldsymbol{v}_h)(\boldsymbol{\tau}^i\cdot\boldsymbol{u}_h)\,\mathrm{d}s + \gamma\int_E {h_e}^{-1}(\boldsymbol{u}_h\cdot\boldsymbol{n})(\boldsymbol{v}_h\cdot\boldsymbol{n})\,\mathrm{d}s + \int_E p'(\boldsymbol{n}\cdot\boldsymbol{v}_h)\,\mathrm{d}s \\
&\qquad+ \int_E q_h(\boldsymbol{n}\cdot\boldsymbol{u}')\,\mathrm{d}s - \int_E \nu\boldsymbol{n}^t D(\boldsymbol{u}')\boldsymbol{n}(\boldsymbol{n}\cdot\boldsymbol{v}_h)\,\mathrm{d}s - \int_E \nu\boldsymbol{n}^t D(\boldsymbol{v}_h)\boldsymbol{n}(\boldsymbol{n}\cdot\boldsymbol{u}')\,\mathrm{d}s\Big) \\
&\qquad+ \sum_{K\in\mathcal{K}_h}((\nabla(q_h),\boldsymbol{u}')_K - (p',\nabla\cdot\boldsymbol{v}_h)_K + (\boldsymbol{u}_h\cdot\nabla\boldsymbol{u}',\boldsymbol{v}_h)_K + (\boldsymbol{u}'\cdot\nabla\boldsymbol{u}_h,\boldsymbol{v}_h)_K + (\boldsymbol{u}'\cdot\nabla\boldsymbol{u}',\boldsymbol{v}_h)_K)
\end{aligned}$$

Now, substitute the values of the fine scale components and this results into the semi-discrete VMS-LES formulation of the Navier–Stokes equation with Nitsche which is expressed in terms of the weak residual as follows: for all $t\in(0,T]$, Find $\boldsymbol{U}_h=\{\boldsymbol{u}_h,p_h\}\in\mathcal{V}_0^h$ with $\boldsymbol{u}_h(\boldsymbol{0})=\boldsymbol{0}$ such that

$$\boldsymbol{H}[\boldsymbol{V}_h;\boldsymbol{U}_h]=\boldsymbol{L}(\boldsymbol{V}_h) \tag{61}$$

for all $\boldsymbol{V}_h=\{\boldsymbol{v}_h,q_h\}\in\mathcal{V}_0^h$, where we considered the following definitions:

$$\begin{aligned}
&\boldsymbol{H}[\boldsymbol{V}_h;\boldsymbol{U}_h] \coloneqq \mathcal{G}^{NS}(\boldsymbol{V}_h,\boldsymbol{U}_h) + \mathcal{G}^{\mathrm{SUPG}}(\boldsymbol{V}_h,\boldsymbol{U}_h) + \mathcal{G}^{\mathrm{VMS}}(\boldsymbol{V}_h,\boldsymbol{U}_h) + \mathcal{G}^{\mathrm{LES}}(\boldsymbol{V}_h,\boldsymbol{U}_h),\\
&\boldsymbol{L}(\boldsymbol{V}_h) \coloneqq \langle\boldsymbol{v}_h,\boldsymbol{f}\rangle_\Omega,
\end{aligned}$$

with

$$\begin{aligned}
\mathcal{G}^{NS}(\boldsymbol{V}_h,\boldsymbol{U}_h) = &\sum_{K\in\mathcal{K}_h}\Big((\partial_t\boldsymbol{u}_h,\boldsymbol{v}_h)_K + \frac{\nu}{2}(D(\boldsymbol{v}_h),D(\boldsymbol{u}_h))_K + (\boldsymbol{v}_h,\boldsymbol{u}_h\cdot\nabla\boldsymbol{u}_h)_K \\
&-(\nabla\cdot\boldsymbol{v}_h,p_h)_K - (q_h,\nabla\cdot\boldsymbol{u}_h)_K) \\
&+ \sum_{E\in\mathcal{E}_{\mathrm{Nav}}}\Big(-\int_E\boldsymbol{n}^t(\nu D(\boldsymbol{u}_h)-p_hI)\boldsymbol{n}(\boldsymbol{n}\cdot\boldsymbol{v}_h)\,\mathrm{d}s - \int_E\boldsymbol{n}^t(\nu D(\boldsymbol{v}_h)-q_hI)\boldsymbol{n}(\boldsymbol{n}\cdot\boldsymbol{u}_h)\,\mathrm{d}s \\
&+ \int_E\beta\sum_i^{d-1}(\boldsymbol{\tau}^i\cdot\boldsymbol{v}_h)(\boldsymbol{\tau}^i\cdot\boldsymbol{u}_h)\,\mathrm{d}s + \gamma\int_E {h_e}^{-1}(\boldsymbol{u}_h\cdot\boldsymbol{n})(\boldsymbol{v}_h\cdot\boldsymbol{n})\,\mathrm{d}s\Big)
\end{aligned} \tag{62}$$

$$\mathcal{G}^{\mathrm{SUPG}}(\boldsymbol{V}_h,\boldsymbol{U}_h) = \sum_{K\in\mathcal{K}_h}\Big(\big(\boldsymbol{u}_h\cdot\nabla\boldsymbol{v}_h - \tilde{C}\nabla q_h,\mathcal{S}_M(\boldsymbol{u}_h)\boldsymbol{r}_M(\boldsymbol{u}_h,p_h)\big)_K + (\nabla\cdot\boldsymbol{v}_h,\mathcal{S}_C(\boldsymbol{u}_h)\boldsymbol{r}_C(\boldsymbol{u}_h))_K\Big) \tag{63}$$

$$\begin{aligned}
\mathcal{G}^{\mathrm{VMS}}(\boldsymbol{V}_h,\boldsymbol{U}_h) = &\sum_{K\in\mathcal{K}_h}\Big(\big(\boldsymbol{u}_h\cdot(\nabla\boldsymbol{v}_h)^T,\mathcal{S}_M(\boldsymbol{u}_h)\boldsymbol{r}_M(\boldsymbol{u}_h,p_h)\big)_K - \sum_{E\in\mathcal{E}_{\mathrm{Nav}}}\Big(\int_E\mathcal{S}_C(\boldsymbol{u}_h)\boldsymbol{r}_C(\boldsymbol{u}_h)(\boldsymbol{n}\cdot\boldsymbol{v}_h)\,\mathrm{d}s \\
&+ \int_E q_h(\boldsymbol{n}\cdot\mathcal{S}_M(\boldsymbol{u}_h)\boldsymbol{r}_M(\boldsymbol{u}_h,p_h))\,\mathrm{d}s - \int_E\nu\boldsymbol{n}^tD(\mathcal{S}_M(\boldsymbol{u}_h)\boldsymbol{r}_M(\boldsymbol{u}_h,p_h))\boldsymbol{n}(\boldsymbol{n}\cdot\boldsymbol{v}_h)\,\mathrm{d}s && (64)\\
&- \int_E\nu\boldsymbol{n}^tD(\boldsymbol{v}_h)\boldsymbol{n}(\boldsymbol{n}\cdot\mathcal{S}_M(\boldsymbol{u}_h)\boldsymbol{r}_M(\boldsymbol{u}_h,p_h))\,\mathrm{d}s\Big) && (65)
\end{aligned}$$

$$\mathcal{G}^{\mathrm{LES}}(\boldsymbol{V}_h,\boldsymbol{U}_h) = -\sum_{K\in\mathcal{K}_h}\Big((\nabla\boldsymbol{v}_h,\mathcal{S}_M(\boldsymbol{u}_h)\boldsymbol{r}_M(\boldsymbol{u}_h,p_h)\otimes\mathcal{S}_M(\boldsymbol{u}_h)\boldsymbol{r}_M(\boldsymbol{u}_h,p_h))_K\Big). \tag{66}$$

In our formulation, we introduce an additional constant $\tilde{C}$ in (63) to discuss two choices for finite element. Expressly, we set $\tilde{C} = 0$ when we use $\mathbb{P}_2 - \mathbb{P}_1$ inf-sup stable finite element. Conversely, when we use stabilized equal order finite element for both the velocity and pressure variables, we set $\tilde{C} = 1$, as stated in [3]. We highlight that (62) represents the weak formulation of the Navier–Stokes equation with Nitsche. Subsequently, (63) represents the classical Streamline Upwind Petrov Galerkin (SUPG) stabilization terms and (65) captures additional terms introduced by the VMS (Variational Multiscale) method. Finally, (66) models the Reynolds stress, which realizes the LES modeling of turbulence.

Remark 4. This formulation differs from the standard one because of the contribution of normal component of the traction vector on the boundary Γ_{Nav}.

Remark 5. It is observed that as the time step Δt approaches zero, the stabilization parameters in (59) behave as follows:

$$\mathcal{S}_M \sim \Delta t \to 0 \quad \mathcal{S}_C \sim \frac{1}{\Delta t} \to \infty.$$

Similar behavior is also demonstrated in [51] *i.e.*, the VMS-LES modeling may lose its effectiveness for small time steps. It is observed that as $\Delta t \to 0$, the term associated with the LES modeling of turbulence $(\nabla \boldsymbol{v}_h, \mathcal{S}_M(\boldsymbol{u}_h)\boldsymbol{r}_M(\boldsymbol{u}_h, p_h) \otimes \mathcal{S}_M(\boldsymbol{u}_h)\boldsymbol{r}_M(\boldsymbol{u}_h, p_h))_K$ becomes negligible, while the dominant term $(\nabla \cdot \boldsymbol{v}_h, \mathcal{S}_C(\boldsymbol{u}_h)\boldsymbol{r}_C(\boldsymbol{u}_h))_K$ fails to effectively act as a turbulence model in the semi-discrete VMS-LES weak formulation of the Navier–Stokes equations (61).

5.2. Time discretization

The time discretization of the problem is formulated according to the Backward Differentiation Formulas (BDF) [49] of order σ. Let us consider a partition of the time domain $(0, T)$ into N subintervals of equal size $\Delta t = \frac{T}{N}$. The subscript n denotes the time step, such that $n = 0, 1, \ldots, N$ and $\Delta t = t_{n+1} - t_n$. We write the approximation of the time derivative as:

$$\partial_t u_h \approx \frac{\alpha_\sigma u_h^{n+1} - u_h^{n,\text{BDF}\sigma}}{\Delta t}.$$

Then, we define $\boldsymbol{u}_h^{n,\text{BDF}\sigma}$ as follow:

$$\boldsymbol{u}_h^{n,\text{BDF}\sigma} = \begin{cases} \boldsymbol{u}_h^n & \text{for } \sigma = 1, \ \text{if } n \geq 1 \quad \text{(BDF1)} \\ 2\boldsymbol{u}_h^n - \frac{1}{2}\boldsymbol{u}_h^{n-1} & \text{for } \sigma = 2, \ \text{if } n \geq 2 \quad \text{(BDF2)} \\ 3\boldsymbol{u}_h^n - \frac{3}{2}\boldsymbol{u}_h^{n-1} + \frac{1}{3}\boldsymbol{u}_h^{n-2} & \text{for } \sigma = 3, \ \text{if } n \geq 3 \quad \text{(BDF3)} \end{cases}$$

and α_σ :

$$\alpha_\sigma = \begin{cases} 1 & \text{for } \sigma = 1 \quad \text{(BDF1)} \\ \frac{3}{2} & \text{for } \sigma = 2 \quad \text{(BDF2)} \\ \frac{11}{6} & \text{for } \sigma = 3 \quad \text{(BDF3)} \end{cases}.$$

Therefore, BDF1 corresponds to the Backward Euler scheme. In this work, we choose the semi-implicit method to discretize the non-linear term of the Navier–Stokes equation. In the semi-implicit method, we linearise the convective term and all related terms with the following scheme:

$$(\boldsymbol{v}_h, (\boldsymbol{u}_h^n \cdot \nabla)\boldsymbol{u}_h^{n+1}).$$

The non-linear term is linearised using the Newton-Gregory backward polynomials with a degree equal to the time discretization order, referred to as "extrapolated variables" denoted as $'n+1, \text{EXT}'$. See [15] for further details.

$$\boldsymbol{u}_h^{n+1,\mathrm{EXT}} = \begin{cases} \boldsymbol{u}_h^n & \text{for } \sigma = 1, \text{ if } n \geq 0 \quad (\mathrm{BDF1}) \\ 2\boldsymbol{u}_h^n - \boldsymbol{u}_h^{n-1} & \text{for } \sigma = 2, \text{ if } n \geq 1 \quad (\mathrm{BDF2}) \\ 3\boldsymbol{u}_h^n - 3\boldsymbol{u}_h^{n-1} + \boldsymbol{u}_h^{n-2} & \text{for } \sigma = 3, \text{ if } n \geq 2 \quad (\mathrm{BDF3}), \end{cases}$$

$$p_h^{n+1,\mathrm{EXT}} = \begin{cases} p_h^n & \text{for } \sigma = 1, \text{ if } n \geq 0 \quad (\mathrm{BDF1}) \\ 2p_h^n - p_h^{n-1} & \text{for } \sigma = 2, \text{ if } n \geq 1 \quad (\mathrm{BDF2}) \\ 3\boldsymbol{p}_h^n - 3\boldsymbol{p}_h^{n-1} + \boldsymbol{p}_h^{n-2} & \text{for } \sigma = 3, \text{ if } n \geq 2 \quad (\mathrm{BDF3}). \end{cases}$$

5.3. Fully discrete VMS-LES formulation

We obtain a fully discrete VMS-LES Nitsche weak formulation of the Navier–Stokes equations by using the BDF and a semi-implicit discretization scheme. Given $\boldsymbol{u}_h^n, \ldots, \boldsymbol{u}_h^{n+1-\sigma}$ for any $n = 0, 1, \ldots N-1$, Find $\boldsymbol{U}_h = \{\boldsymbol{u}_h^{n+1}, p_h^{n+1}\} \in \mathcal{V}_0^h$:

$$\tilde{\mathcal{G}}^{NS}(\boldsymbol{V}_h, \boldsymbol{U}_h) + \tilde{\mathcal{G}}^{\mathrm{SUPG}}(\boldsymbol{V}_h, \boldsymbol{U}_h) + \tilde{\mathcal{G}}^{\mathrm{VMS}}(\boldsymbol{V}_h, \boldsymbol{U}_h) + \tilde{\mathcal{G}}^{\mathrm{LES}}(\boldsymbol{V}_h, \boldsymbol{U}_h) = \langle \boldsymbol{v}_h, \boldsymbol{f}^{n+1} \rangle_\Omega, \tag{67}$$

for all $\boldsymbol{V}_h = \{\boldsymbol{v}_h, q_h\} \in \mathcal{V}_0^h$, for all $n \geq \sigma - 1$ with $\boldsymbol{f}^{n+1} = \boldsymbol{f}(t^{n+1})$.

The bilinear forms $\tilde{\mathcal{G}}^{NS}(\boldsymbol{V}_h, \boldsymbol{U}_h), \tilde{\mathcal{G}}^{\mathrm{SUPG}}(\boldsymbol{V}_h, \boldsymbol{U}_h), \tilde{\mathcal{G}}^{\mathrm{VMS}}(\boldsymbol{V}_h, \boldsymbol{U}_h)$, and $\tilde{\mathcal{G}}^{\mathrm{LES}}(\boldsymbol{V}_h, \boldsymbol{U}_h)$ are defined below. These forms are modifications of the bilinear forms defined in (61).

$$\begin{aligned}
\tilde{\mathcal{G}}^{NS}(\boldsymbol{V}_h, \boldsymbol{U}_h) \coloneqq \sum_{K \in \mathcal{K}_h} \Bigg(&\left(\left(\boldsymbol{v}_h, \frac{\alpha_\sigma \boldsymbol{u}_h^{n+1} - \boldsymbol{u}_h^{n,\mathrm{BDF}\sigma}}{\Delta t}\right)_K + \left(\boldsymbol{v}_h, \boldsymbol{u}_h^{n+1,\mathrm{EXT}} \cdot \nabla \boldsymbol{u}_h^{n+1}\right)_K + \frac{\nu}{2}\left(D(\boldsymbol{v}_h), D(\boldsymbol{u}_h^{n+1})\right)_K \right. \\
&\left. - \left(\nabla \cdot \boldsymbol{v}_h, p_h^{n+1}\right)_K - \left(q_h, \nabla \cdot \boldsymbol{u}_h^{n+1}\right)_K\right) + \sum_{E \in \mathcal{E}_h^b} \left(- \int_E \boldsymbol{n}^t \left(\nu D(\boldsymbol{u}_h^{n+1}) - p_h^{n+1} I\right) \boldsymbol{n}(\boldsymbol{n} \cdot \boldsymbol{v}_h) \,\mathrm{d}s\right. \\
&- \int_E \boldsymbol{n}^t (\nu D(\boldsymbol{v}_h) - q_h I) \boldsymbol{n}\left(\boldsymbol{n} \cdot \boldsymbol{u}_h^{n+1}\right) \mathrm{d}s + \int_E \beta \sum_i^{d-1} \left(\boldsymbol{\tau}^i \cdot \boldsymbol{v}_h\right)\left(\boldsymbol{\tau}^i \cdot \boldsymbol{u}_h^{n+1}\right) \mathrm{d}s \\
&\left. + \gamma \int_E {h_e}^{-1} \left(\boldsymbol{u}_h^{n+1} \cdot \boldsymbol{n}\right)(\boldsymbol{v}_h \cdot \boldsymbol{n}) \,\mathrm{d}s\right)
\end{aligned}$$

$$\begin{aligned}
\tilde{\mathcal{G}}^{\mathrm{SUPG}}(\boldsymbol{V}_h, \boldsymbol{U}_h) \coloneqq \sum_{K \in \mathcal{K}_h} \Bigg(&\left(\boldsymbol{u}_h^{n+1,\mathrm{EXT}} \cdot \nabla \boldsymbol{v}_h - \tilde{C} \nabla q_h, \mathcal{S}_M\left(\boldsymbol{u}_h^{n+1,\mathrm{EXT}}\right) \boldsymbol{r}_M\left(\boldsymbol{u}_h^{n+1}, p_h^{n+1}\right)\right)_K \\
&+ \left(\nabla \cdot \boldsymbol{v}_h, \mathcal{S}_C\left(\boldsymbol{u}_h^{n+1,\mathrm{EXT}}\right) r_C\left(\boldsymbol{u}_h^{n+1}\right)\right)_K \Bigg) \\
\tilde{\mathcal{G}}^{\mathrm{VMS}}(\boldsymbol{V}_h, \boldsymbol{U}_h) \coloneqq \sum_{K \in \mathcal{K}_h} &\left(\boldsymbol{u}_h^{n+1,\mathrm{EXT}} \cdot (\nabla \boldsymbol{v}_h)^T, \mathcal{S}_M\left(\boldsymbol{u}_h^{n+1,\mathrm{EXT}}\right) \boldsymbol{r}_M\left(\boldsymbol{u}_h^{n+1}, p_h^{n+1}\right)\right)_K \\
- \sum_{E \in \mathcal{E}_h^b} &\left(\int_E \mathcal{S}_C\left(\boldsymbol{u}_h^{n+1,\mathrm{EXT}}\right) \boldsymbol{r}_C\left(\boldsymbol{u}_h^{n+1}\right)(\boldsymbol{n} \cdot \boldsymbol{v}_h) \,\mathrm{d}s \right. \\
&+ \int_E q_h \left(\boldsymbol{n} \cdot \mathcal{S}_M\left(\boldsymbol{u}_h^{n+1,\mathrm{EXT}}\right) \boldsymbol{r}_M\left(\boldsymbol{u}_h^{n+1}, p_h^{n+1}\right)\right) \mathrm{d}s \\
&- \int_E \nu \boldsymbol{n}^t D\left(\mathcal{S}_M\left(\boldsymbol{u}_h^{n+1,\mathrm{EXT}}\right) \boldsymbol{r}_M\left(\boldsymbol{u}_h^{n+1}, p_h^{n+1}\right)\right) \boldsymbol{n}(\boldsymbol{n} \cdot \boldsymbol{v}_h) \,\mathrm{d}s \\
&\left. - \int_E \nu \boldsymbol{n}^t D(\boldsymbol{v}_h) \boldsymbol{n}\left(\boldsymbol{n} \cdot \mathcal{S}_M\left(\boldsymbol{u}_h^{n+1,\mathrm{EXT}}\right) \boldsymbol{r}_M\left(\boldsymbol{u}_h^{n+1}, p_h^{n+1}\right)\right) \mathrm{d}s \right)
\end{aligned}$$

$$\tilde{\mathcal{G}}^{\,\mathrm{LES}}\left(\boldsymbol{V}_h,\boldsymbol{U}_h\right) := -\sum_{K\in\mathcal{K}_h}\left(\nabla\boldsymbol{v}_h,\mathcal{S}_M\left(\boldsymbol{u}_h^{n+1,\mathrm{EXT}}\right)\boldsymbol{r}_M\left(\boldsymbol{u}_h^{n+1,\mathrm{EXT}},p_h^{n+1,\mathrm{EXT}}\right)\right.$$
$$\left.\otimes\,\mathcal{S}_M\left(\boldsymbol{u}_h^{n+1,\mathrm{EXT}}\right)\boldsymbol{r}_M\left(\boldsymbol{u}_h^{n+1},p_h^{n+1}\right)\right)_K$$

The extrapolated residual and the stabilization parameters for this formulation are defined as:

$$\boldsymbol{r}_M\left(\boldsymbol{u}_h^{n+1},p_h^{n+1}\right) = \frac{\alpha_\sigma \boldsymbol{u}_h^{n+1}}{\Delta t} + \boldsymbol{u}_h^{n+1,\mathrm{EXT}}\cdot\nabla\boldsymbol{u}_h^{n+1} + \nabla p_h^{n+1} - \nu\Delta\boldsymbol{u} - \frac{\boldsymbol{u}_h^{n,\mathrm{BDF}\sigma}}{\Delta t} - \boldsymbol{f}^{n+1},$$
$$\mathcal{S}_M\left(\boldsymbol{u}_h^{n+1,\mathrm{EXT}}\right) = \left(\frac{\sigma^2}{\Delta t^2} + \boldsymbol{u}_h^{n+1,\mathrm{EXT}}\cdot\boldsymbol{G}\boldsymbol{u}_h^{n+1,\mathrm{EXT}} + C_r\nu^2\boldsymbol{G}:\boldsymbol{G}\right)^{-1/2},$$
$$\mathcal{S}_C\left(\boldsymbol{u}_h^{n+1,\mathrm{EXT}}\right) = \left(\mathcal{S}_M\left(\boldsymbol{u}_h^{n+1,\mathrm{EXT}}\right)\boldsymbol{g}\cdot\boldsymbol{g}\right)^{-1}.$$

6. Numerical tests

Computational examples are now presented to validate the numerical scheme. All numerical computations are performed using the open-source finite element library FEniCS [1] and plotted with Paraview [36]. We present three tests: convergence tests (Test 1), lid-driven cavity test (Test 2), and the flow past through a circular cylinder (Test 3). A Lagrange multiplier is used to implement the average zero condition for the pressure approximation.

6.1. Test 1: convergence tests against manufactured solutions

6.1.1. Convergence test for Nitsche scheme (stationary)

In this numerical test, we approximate the velocity and pressure by Taylor-Hood element $\mathbb{P}_2-\mathbb{P}_1$ and compute the convergence rate for the Nitsche method described in Section 3. Consider the square domain $\Omega = (-1,1)^2$ and a sequence of uniformly refined meshes. We present a numerical test based on the following exact solution.

$$\boldsymbol{u}(x,y) = \left(2y(1-x^2), -2x(1-y^2)\right)^T$$
$$p(x,y) = (2x-1)(2y-1).$$

The slip boundary condition is imposed on $x_2=-1$, and the essential boundary condition is enforced on rest of the boundary. We can observe that Table 1 presents the approximation errors for pressure and velocity as well as the convergence rate, which are in good agreement with the theory. Table 2 gives the error in L^2 norm on the slip condition on Γ_{Nav} and it shows that the larger the Nitsche parameter γ is, the smaller error on the slip condition. Additionally, we see that the number of Newton iterations required to reach the prescribed tolerance of 10^{-7} is at most three. The velocity field computed at $\nu=1$ is depicted on the left-hand side of Figure 1 with $\beta=10$ and $\gamma=10$.

Remark 6. We note that we did not experience conditioning issues during the development of our numerical tests. This is on one hand due to the use of direct solvers, but another more interesting point is that it has been shown for the Laplace operator that the Nitsche formulation maintains the conditioning of the system [35]. This is not the case for penalty methods, and we believe that a similar behavior could be shown for this problem.

6.1.2. Convergence test for VMS-LES Nitsche scheme (unsteady)

In this numerical test, we approximate the velocity and pressure by stabilized finite element $\mathbb{P}_1-\mathbb{P}_1$ and compute the convergence rate for the VMS-LES Nitsche scheme described in Section 5.3. The accuracy of the spatio-temporal discretization is verified using the exact solution from [12], defined on the domain $\Omega=(0,1)^2$:

$$\boldsymbol{u}(x,y) = \left(\sin(\pi x-0.6)\sin(\pi y+0.22)\cos(t), \cos(\pi x-0.6)\cos(\pi y+0.22)\cos(t)\right)^T,$$

TABLE 1. Test 1: experimental errors, iteration count, number of degree of freedom (D.O.F.), and convergence rates for the approximate solutions $\boldsymbol{u}_h$ and p_h. Values are displayed for Taylor–Hood space $\mathbb{P}_2 - \mathbb{P}_1$ with $\beta = 10$ and $\nu = 1$.

γ	Mesh	D.O.F.	Newton Its	$\|p - p_h\|_0$	Rate	$\|\nabla(\boldsymbol{u} - \boldsymbol{u}_h)\|$	Rate	$\|\boldsymbol{u} - \boldsymbol{u}_h\|_0$	Rate
1.0	8×8	659	3	5.20×10^{-2}	–	1.12×10^{-1}	–	4.90×10^{-3}	–
	16×16	2467	2	1.27×10^{-2}	2.03	2.23×10^{-2}	2.32	4.90×10^{-4}	3.34
	32×32	9539	2	3.13×10^{-3}	2.02	4.55×10^{-3}	2.29	5.00×10^{-5}	3.30
	64×64	37 507	2	7.78×10^{-4}	2.01	1.23×10^{-3}	1.88	7.00×10^{-6}	2.92
	128×128	148 739	2	1.94×10^{-4}	2.00	2.59×10^{-4}	2.25	1.00×10^{-6}	3.23
10	8×8	659	3	5.18×10^{-2}	–	8.33×10^{-2}	–	3.47×10^{-3}	–
	16×16	2467	2	1.27×10^{-2}	2.02	1.81×10^{-2}	2.19	3.82×10^{-4}	3.18
	32×32	9539	2	3.14×10^{-3}	2.02	4.24×10^{-3}	2.10	4.50×10^{-5}	3.09
	64×64	37 507	2	7.78×10^{-4}	2.01	1.03×10^{-3}	2.04	5.00×10^{-6}	3.04
	128×128	148 739	2	1.94×10^{-4}	2.00	2.53×10^{-4}	2.02	1.00×10^{-6}	3.01
100	8×8	659	3	5.15×10^{-2}	–	6.32×10^{-2}	–	2.74×10^{-3}	–
	16×16	2467	2	1.27×10^{-2}	2.02	1.59×10^{-2}	1.98	3.42×10^{-4}	3.00
	32×32	9539	2	3.13×10^{-3}	2.02	3.90×10^{-3}	1.99	4.30×10^{-5}	3.00
	64×64	37 507	2	7.78×10^{-4}	2.01	1.00×10^{-3}	1.99	5.00×10^{-6}	2.99
	128×128	148 739	2	1.94×10^{-4}	2.00	2.50×10^{-4}	1.99	1.00×10^{-6}	2.99

TABLE 2. Test 1: computation of $\|\boldsymbol{u}_h \cdot \boldsymbol{n}\|_{0,\Gamma_{\mathrm{Nav}}}$ for different values of γ.

Mesh	$\gamma = 0.01$	$\gamma = 0.1$	$\gamma = 1$	$\gamma = 10$	$\gamma = 100$
8×8	1.09×10^{-2}	1.10×10^{-2}	1.87×10^{-2}	1.31×10^{-2}	5.77×10^{-4}
16×16	1.32×10^{-3}	1.37×10^{-3}	2.23×10^{-3}	1.46×10^{-3}	6.40×10^{-5}
32×32	2.16×10^{-4}	7.35×10^{-4}	2.24×10^{-4}	1.60×10^{-4}	7.00×10^{-6}
64×64	2.20×10^{-5}	1.90×10^{-5}	4.90×10^{-5}	1.80×10^{-5}	1.00×10^{-6}
128×128	3.00×10^{-6}	3.00×10^{-6}	2.00×10^{-6}	2.00×10^{-6}	1.00×10^{-7}

$$p(x, y) = \cos(t)(\sin x \cos y + (\cos(1) - 1)\sin(1)),$$

with $\nu = 3.571 \times 10^{-6}$. We also choose $\beta = 1$ and $\gamma = 10$, and the right-hand side datum $\boldsymbol{f}$ is manufactured using these closed-form solutions. We verify convergence in space and time separately using the following time-discrete norms:

$$\|e_{\boldsymbol{u}}\|_{l^2(\boldsymbol{L}^2)} := \Delta t \sum_{n=1}^{N} \|\boldsymbol{u}(t_{n+1}) - \boldsymbol{u}_h^{n+1}\|^2_{\boldsymbol{L}^2(\Omega)} \text{ and } \|e_{\boldsymbol{u}}\|_{l^2(\boldsymbol{H}^1)} := \Delta t \sum_{n=1}^{N} \|\boldsymbol{u}(t_{n+1}) - \boldsymbol{u}_h^{n+1}\|^2_{\boldsymbol{H}^1(\Omega)},$$
$$\|e_p\|_{l^2(L^2)} := \Delta t \sum_{n=1}^{N} \|p(t_{n+1}) - p_h^{n+1}\|^2_{L^2(\Omega)}.$$

For the space convergence, we generate successively refined simplicial grids and use a sufficiently small time step $\Delta t = 0.001$ and simulate a relatively short time horizon $T = 0.01$ to guarantee that the error produced by the time discretization does not dominate. Errors between the approximate and exact solutions are tabulated against the number of degrees of freedom in Table 3. This error history confirms the optimal convergence of the finite element scheme for both velocity and pressure.

The convergence in time achieved by the backward Euler method is verified by partitioning the time interval $(0, 1)$ into successively refined uniform discretizations and computing accumulated errors for velocity and pres-

TABLE 3. Experimental errors related to spatial discretization and convergence rates are computed for the approximate solutions $\boldsymbol{u}_h$ and p_h, using stabilized finite element $\mathbb{P}_1 - \mathbb{P}_1$. The computations are performed at the last time step.

D.O.F.	h	$\\|e_{\boldsymbol{u}}\\|_{l^2(\boldsymbol{L}^2)}$	Rate	$\\|e_{\boldsymbol{u}}\\|_{l^2(\boldsymbol{H}^1)}$	Rate	$\\|e_p\\|_{l^2(L^2)}$	Rate
76	0.3535	2.16×10^{-2}	–	1.67×10^{-1}	–	1.96×10^{0}	–
244	0.1767	3.93×10^{-3}	2.46	7.26×10^{-2}	1.19	2.65×10^{-1}	2.88
868	0.0883	5.72×10^{-4}	2.73	3.21×10^{-2}	1.17	3.72×10^{-2}	2.83
3268	0.0442	1.06×10^{-4}	2.42	1.55×10^{-2}	1.05	6.58×10^{-3}	2.49
12 678	0.0221	2.51×10^{-5}	2.09	7.72×10^{-3}	1.00	1.43×10^{-3}	2.20
49 924	0.0110	6.28×10^{-6}	1.99	3.85×10^{-3}	1.00	3.25×10^{-4}	2.14
198 148	0.0055	1.66×10^{-6}	1.92	1.92×10^{-3}	1.01	7.14×10^{-5}	2.18

TABLE 4. Experimental cumulative errors associated with the temporal discretisation and convergence rates for the approximate solutions $\boldsymbol{u}_h$ and p_h, using a backward Euler scheme (BDF1).

Δt	$\\|e_{\boldsymbol{u}}\\|_{l^2(\boldsymbol{L}^2)}$	Rate	$\\|e_{\boldsymbol{u}}\\|_{l^2(\boldsymbol{H}^1)}$	Rate	$\\|e_p\\|_{l^2(L^2)}$	Rate
0.5	2.37×10^{-2}	–	8.45×10^{-1}	–	4.61×10^{-2}	–
0.225	1.27×10^{-2}	0.89	4.39×10^{-1}	0.94	2.49×10^{-2}	0.88
0.125	6.71×10^{-3}	0.93	2.27×10^{-1}	0.95	1.29×10^{-2}	0.95
0.0625	3.50×10^{-3}	0.94	1.19×10^{-1}	0.93	6.57×10^{-3}	0.97
0.03125	1.79×10^{-3}	0.95	6.83×10^{-2}	0.82	3.31×10^{-3}	0.99

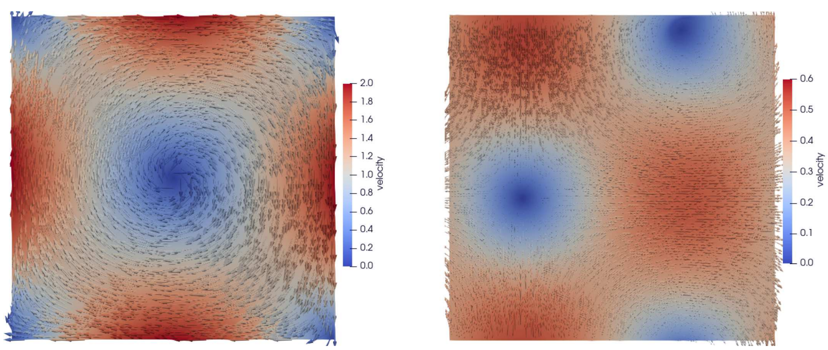

$\nu = 1$ $\nu = 3.571 \times 10^{-6}$

FIGURE 1. Test 1, velocity field.

sure in the time-discrete norms previously defined. For this test, we use a fixed mesh involving 198148 DOFs. The results are shown in Table 4, confirming the optimal first-order convergence. The velocity field computed at $\nu = 3.571 \times 10^{-6}$ is illustrated on the right-hand side of Figure 1, with a final time of $T = 1$ and a time step of $\Delta t = 0.25$, using parameter values $\beta = 1$, and $\gamma = 10$.

6.2. Test 2: lid driven cavity test

We perform a lid-driven cavity test for steady and unsteady formulations. First, consider the stationary Navier–Stokes equations with slip boundary condition. The evaluation includes modeling a planar flow of an

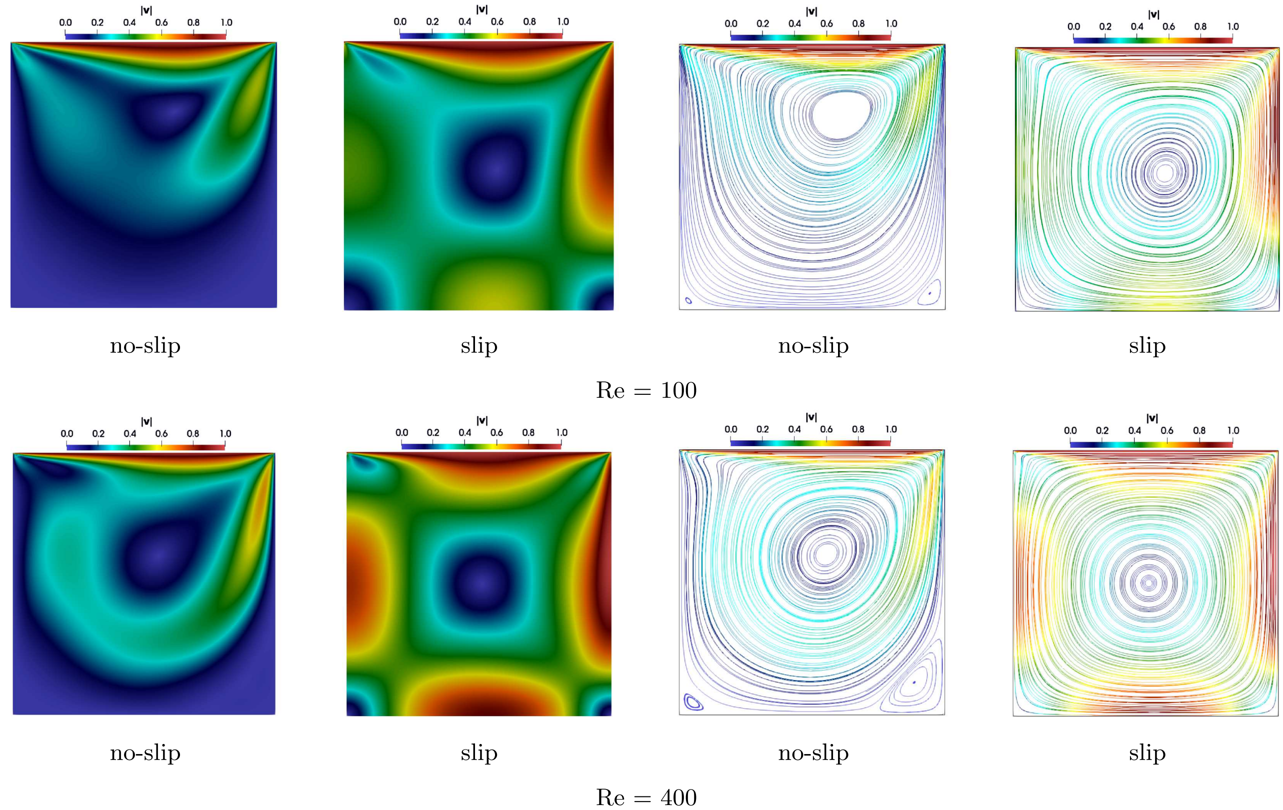

FIGURE 2. Test 2, velocity magnitude and streamlines at $\mathrm{Re} \in \{100, 400\}$ with slip boundary conditions and no-slip at the left, right, and bottom for the stationary case.

isothermal fluid inside a cavity driven. The cavity is represented as a square domain $\Omega = (0,1)^2$, with negligible body force and one moving wall. The velocity imposed on the top boundary $\{y = 1\}$ is defined as $\boldsymbol{u} = (1,0)^{\mathrm{T}}$ and the homogeneous slip boundary with $\beta = 0$ and $\gamma = 10$ is enforced on the other three sides. The Reynolds number is given by the formula $\mathrm{Re} = \frac{UL}{\nu}$ where U represents the average velocity of the fluid in the x direction, and L corresponds to the length of the cavity. We approximate the velocity and pressure by Taylor-Hood element $\mathbb{P}_2 - \mathbb{P}_1$, and the domain is discretized with $h = 1/128$. In Figure 2, the first row shows the velocity magnitude and streamlines at $\mathrm{Re} = 100$ with slip and no-slip boundary conditions. The second row shows the same at $\mathrm{Re} = 400$ with and without slip conditions. It also shows that as the Reynolds number increases, the primary vortex migrates towards the center of the cavity. The results follow the expected behavior and are in agreement with those reported in [14, 46].

Secondly, we consider the unsteady Navier–Stokes equations with slip boundary conditions and apply the VMS-LES Nitsche scheme to simulate high Reynolds numbers. We approximate the velocity and pressure using $\mathbb{P}_1 - \mathbb{P}_1$ finite elements, with the domain discretized at $h = 1/256$, a time step of $\Delta t = 0.1$, and parameters $\beta = 0$ and $\gamma = 10$. The final times are $T = 40$ (for $\mathrm{Re} = 1000$), $T = 192$ (for $\mathrm{Re} = 5000$), and $T = 350$ (for $\mathrm{Re} = 10\,000$). For each value of $\mathrm{Re} \in \{1000, 5000, 10\,000\}$, we compare the streamlines and vortex center positions of the steady-state solutions for the no-slip boundary case with the results reported in [29, 58], as shown in Figures 2 and 3. We also compare these for $\mathrm{Re} \in \{100, 400\}$, as they are the solutions of the steady-state equation. Our results are obtained with a uniform mesh of size $h = 1/256$ and a total number of elements $N = 256 \times 256$, corresponding to $198\,148$ degrees of freedom. We observe that the results with the no-slip

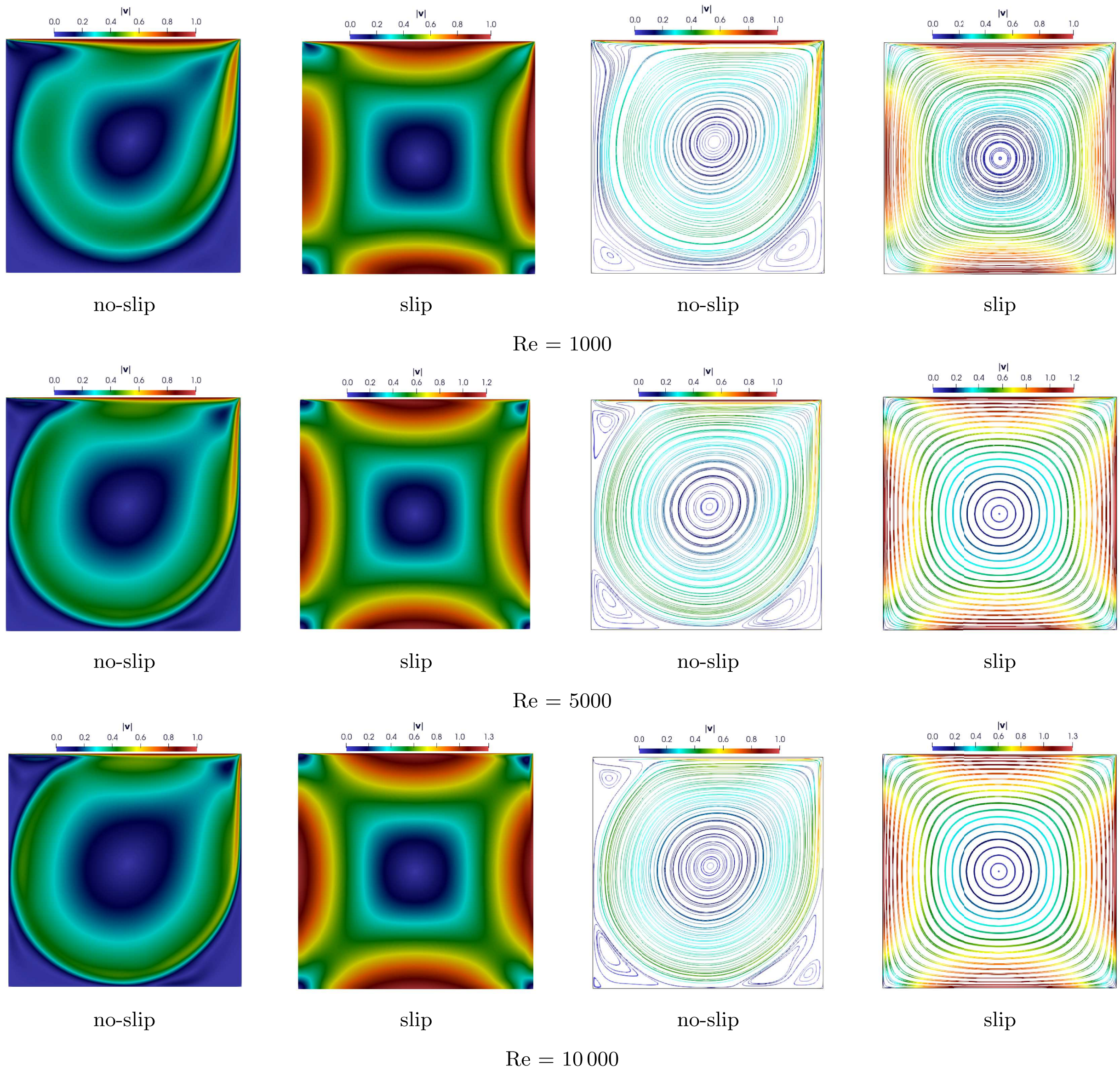

FIGURE 3. Test 2, velocity magnitude and streamlines at Re $\in \{1000, 5000, 10\,000\}$ with slip boundary conditions and no-Slip at the *left*, *right*, and *bottom* for unsteady case.

boundary conditions are qualitatively similar to those reported in [29, 58]; *i.e.*, the number of regions in which the vortices develop increases with the Reynolds number, specifically at the corners of the domain. For example, for Re = 10 000, we can observe in Figure 3 that two secondary vortices appear in the bottom corners and a third vortex appears in the upper right corner. When no-slip conditions are imposed, the stronger inertial forces due to the lid on the top boundary lead to more complex flow patterns as the Reynolds number rises. Interestingly, the freedom provided by the slip condition avoids the formation of such patterns, which suggest that the boundary conditions could play a major role in the formation of vortexes.

The magnitude and streamline plots of steady-state velocity solutions in Figures 2 and 3 demonstrate that the velocity near the boundary increases with the Reynolds number under slip conditions. In the slip case, the viscous forces near the boundaries are reduced, resulting in decreased flow instabilities and, consequently, no formation of secondary vortices with the Reynolds number Thus, Figures 2 and 3 clearly demonstrate the impact of slip boundary conditions on the flow behavior.

We have chosen the lines $(0.5, y)$ and $(x, 0.5)$ and plotted the velocity profile along them. In Figure 4, the plots for the no-slip boundary condition at the discretization $h = 1/128$ (for $\mathrm{Re} \in \{100, 400\}$) and $h = 1/256$ (for $\mathrm{Re} \in \{1000, 5000, 10\,000\}$) are similar to those reported in [29, 58]. The corresponding lines for the slip condition are shown with dotted lines at the same Reynolds numbers, which clearly displays that there is a non-null tangential component of the velocity at the boundary.

6.3. Test 3: flow past through a circular cylinder (Re = 10 000)

This example is based on a standard three-dimensional CFD (computational fluid dynamics) benchmark problem: flow past through a circular cylinder. The geometrical settings of the domain are taken from [2, 7]. The computational mesh is depicted in Figure 5.

In this problem, we impose no-slip boundary conditions on all the lateral walls of the box, and we use do-nothing boundary conditions at the outflow plane. For the surface of the cylinder, we impose the homogeneous slip condition. Finally, the inflow condition from [7] is given by

$$\boldsymbol{u}_D := \left(\frac{16 U_m \sin\left(\frac{\pi}{8} t\right) yz(H-y)(H-z)}{H^4}, 0, 0 \right)^T, \tag{68}$$

with $U_m(t) := 2.25$ m/s and $H = 0.41$ m. The Reynolds number is given by the formula $\mathrm{Re} = \frac{UD}{\nu}$ where U represents the average velocity of the fluid imposed on the inflow boundary, and D corresponds to the diameter of the cylinder. First, we approximate the velocity and pressure by stabilized finite element $\mathbb{P}_1 - \mathbb{P}_1$, and the mesh involving 118729 DOFs. Choose the values of the parameters as follows: $\nu = 1 \times 10^{-5}, \beta = 0$ and $\gamma = 10$. Our aim to study the behavior of the fluid velocity at high Reynolds number ($\mathrm{Re} = 10\,000$) for both slip and no-slip boundary conditions around a circular cylinder. The numerical solution of the fluid velocity at different time intervals, specifically at $T = 4, 6, 8$, using a time step of $\Delta t = 0.01$ are depicted in Figures 6, 7, and 8, respectively.

By Enforcing the no-slip boundary condition around the circular cylinder results in fluid adherence to the boundary, thereby generating frictional forces that significantly influence the fluid flow rate. Furthermore, applying the slip boundary condition a thin slip layer around the cylinder is observed as shown in top Figures of 6–8. Upon comparing the overall flow under both conditions, we observe that the flow velocity is more pronounced with the slip boundary condition in contrast to the no-slip boundary condition. The inflow velocity at $T = 4$, reaches its maximum (see (68)), and the effects due to imposition of slip boundary condition are more noticeable. Conversely, the inflow velocity reaches its minimum at $T = 8$. It is noteworthy to emphasize that, to highlight the effects at $T = 8$, we have narrowed down the range of the corresponding legend. As time progresses from $T = 4$ to $T = 8$, the changes in fluid flow velocities diminish under both slip and no-slip boundary conditions. Nonetheless, slight variations and fluctuations persist due to flow dynamics.

Additionally, we computed difference between the velocity magnitude with slip and without no-slip boundary conditions, as shown in Figure 9. Thus, the change in both boundary conditions occurs only at the boundary of the obstacle (cylinder), but the solution changes globally. Notably, the difference effects are more pronounced at $T = 4$, also seen in flow velocity magnitude in Figure 6. However, as time progresses, particularly from $T = 4$ to $T = 8$, the overall fluid rate effects, and the difference decreases. The numerical solution for the pressure is shown in Figure 10.

We conduct a comparative analysis of the drag coefficient $c_{\mathrm{d}}(t)$, lift coefficients $c_\ell(t)$, and pressure differences $\Delta p(t)$ between the front point $(0.45, 0.2, 0.205)$ and back point $(0.55, 0.2, 0.205)$ of the cylinder over time t. The

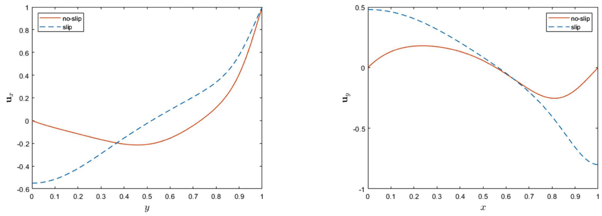

(a)

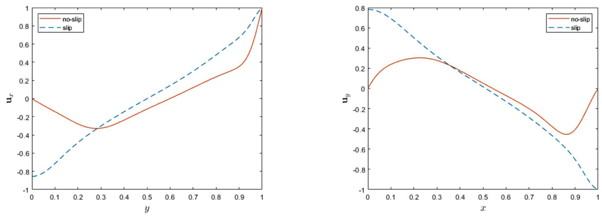

(b)

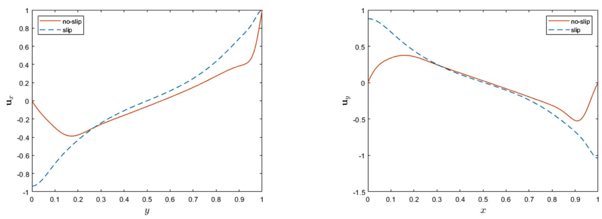

(c)

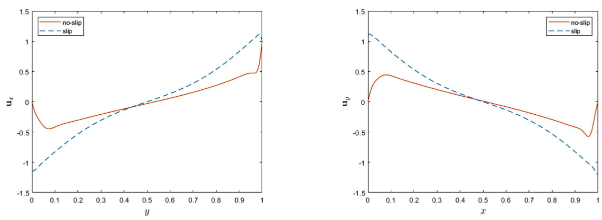

(d)

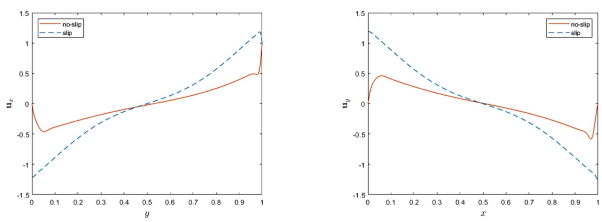

(e)

FIGURE 4. Test 2, velocities computed through the centerlines of the cavity. Horizontal component $\boldsymbol{u}_x$ of the velocity field along the vertical centerline *vs.* the coordinate y (*left*) and vertical component $\boldsymbol{u}_y$ of the velocity field along the horizontal centerline *vs.* the coordinate x (*right*), for different values of the Reynolds number $\mathrm{Re} \in \{100, 400, 1000, 5000, 10\,000\}$ with both slip and no-slip boundary conditions at the left, right, and the bottom. (a) $\mathrm{Re} = 100$. (b) $\mathrm{Re} = 400$. (c) $\mathrm{Re} = 1000$. (d) $\mathrm{Re} = 5000$. (e) $\mathrm{Re} = 10\,000$.

FIGURE 5. Test 3: surface view of the computational mesh.

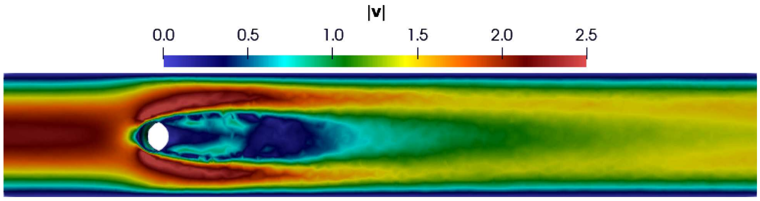

Slip boundary condition on the inner cylinder

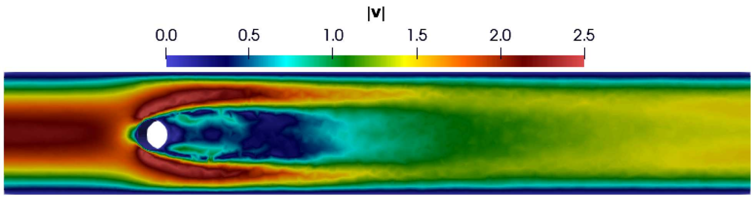

No-slip boundary condition on the inner cylinder

FIGURE 6. Velocity magnitude at $T = 4$.

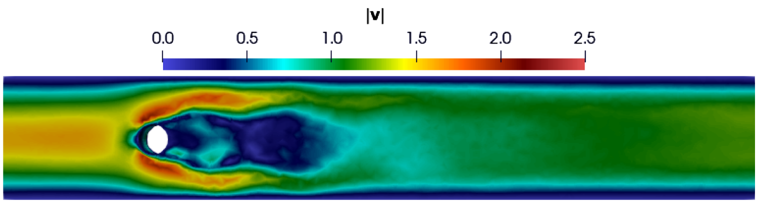

Slip boundary condition on the inner cylinder

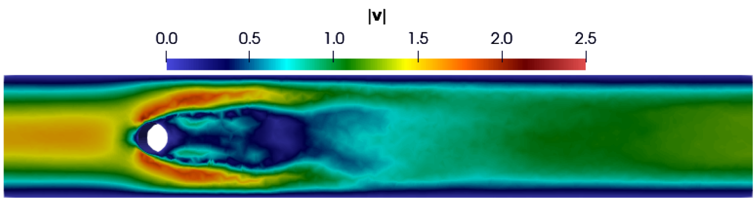

No-slip boundary condition on the inner cylinder

FIGURE 7. Velocity magnitude at $T = 6$.

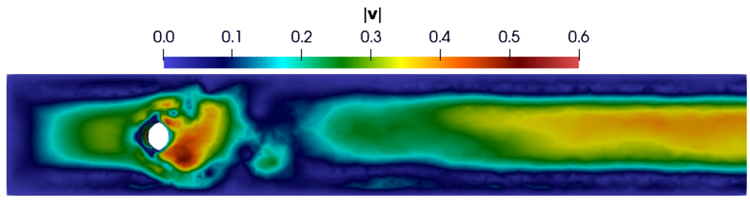

Slip boundary condition on the inner cylinder

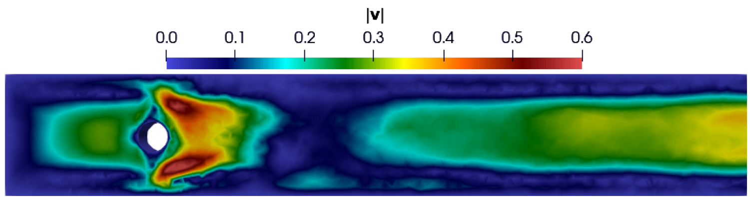

No-slip boundary condition on the inner cylinder

FIGURE 8. Velocity magnitude at $T = 8$.

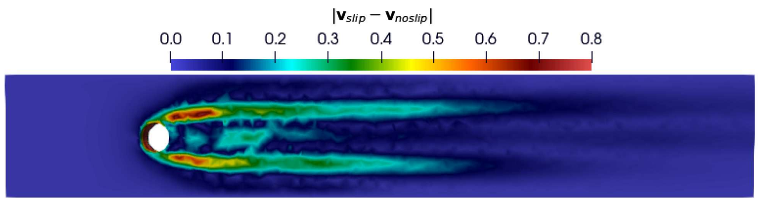

T=4

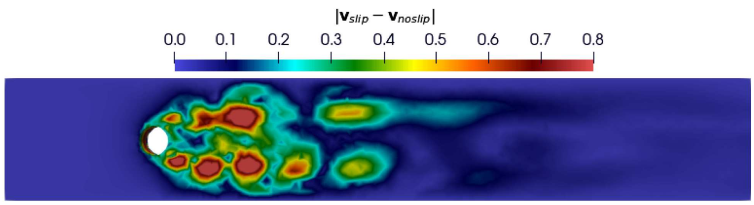

T=6

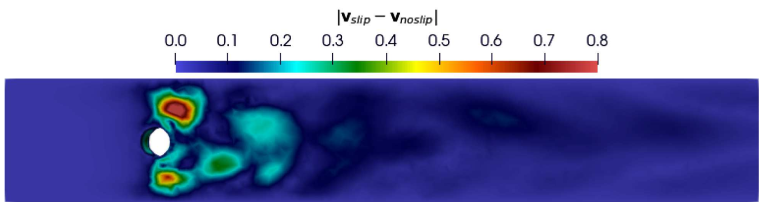

T=8

FIGURE 9. Error between the velocity magnitude of slip and no-slip boundary condition.

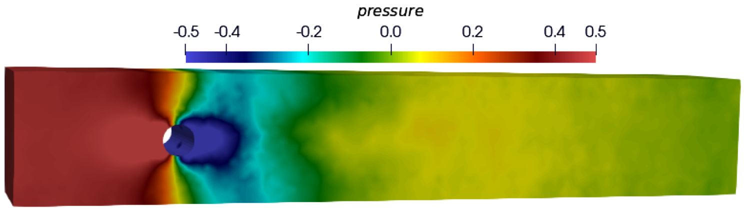

Slip boundary condition on the inner cylinder

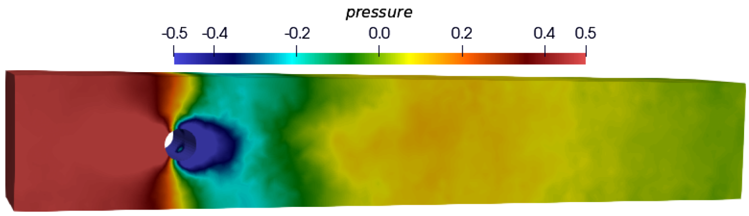

No-slip boundary condition on the inner cylinder

FIGURE 10. Isovalues of pressure at $T = 4$.

dimensionless drag and lift coefficients for the cylinder taken from [63, 64] are calculated as

$$c_{\mathrm{d}} = \frac{2F_{\mathrm{d}}}{U^2 DH}, \quad c_\ell = \frac{2F_\ell}{U^2 DH}$$

where F_{d} and F_ℓ are defined as,

$$F_{\mathrm{d}} = \int_S \left(\nu \frac{\partial \boldsymbol{u}_{\tau_1}}{\partial \boldsymbol{n}_S} n_y - p n_x \right) \mathrm{d}s, \quad F_\ell = -\int_S \left(\nu \frac{\partial \boldsymbol{u}_{\tau_1}}{\partial \boldsymbol{n}_S} n_x + p n_y \right) \mathrm{d}s$$

with the following notation: surface of the cylinder S, $\boldsymbol{n}_S = (n_x, n_y, 0)$ be the inward pointing unit normal with respect to Ω and the tangent vectors are $\tau_1 = (n_y, -n_x, 0)$ and $\tau_2 = (0, 0, 1)$. This analysis involves studying scenarios with slip and no-slip boundary conditions applied at the inner cylinder's boundary, as depicted in Figure 11. In the slip case, we observe a lower drag coefficient, a higher lift coefficient, and a reduced pressure difference, which indicate a more efficient flow around the cylinder compared to the non-slip case. We also focus on the highest values of the drag coefficient, lift coefficient, and the final value of the pressure difference.

7. Conclusion

In this paper, we address two main contributions. Firstly, we analyze Nitsche's method for the stationary Navier–Stokes equations on Lipschitz polygonal domains. Our analysis provides a robust formulation for implementing slip (*i.e.*, Navier) boundary conditions on arbitrarily complex boundaries. We establish the well-posedness of the discrete problem using the Banach Neas Babuka and the Banach fixed-point theorems under standard small data assumptions, and we provide optimal convergence rates for the approximation error. Secondly, we propose the utility of the VMS-LES stabilized scheme within the Nitsche formulation to validate the simulation of incompressible fluids at high Reynolds numbers. In the numerical part, optimal convergence rates have been shown for both Nitsche and VMS-LES Nitsche schemes. Moreover, the results of computational experiments on two benchmark problems show that the proposed method works well for arbitrarily Reynolds numbers. We also compare the results with slip and no-slip boundary conditions, which validates the application of slip conditions.

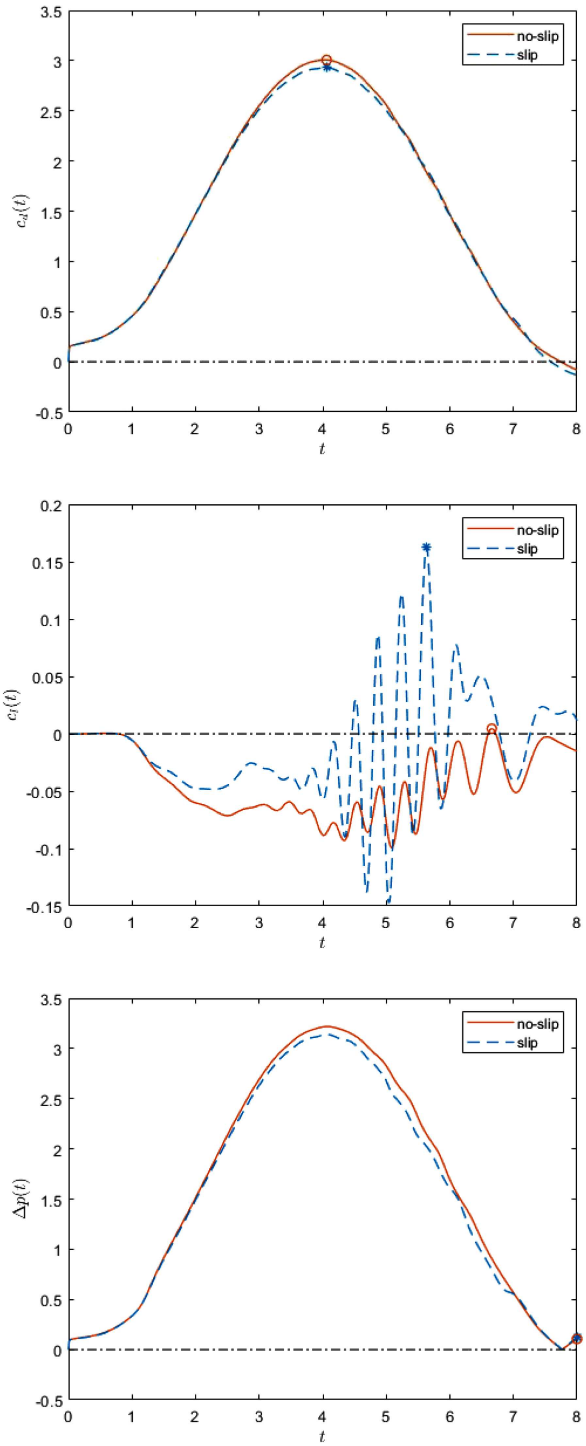

FIGURE 11. Test 3, drag coefficient, lift coefficient, and pressure difference.

Acknowledgements

We thank the referees for the careful reading of the manuscript and their valuable suggestions.

Funding

AB was supported by the Ministry of Education, Government of India – MHRD for financial assistance. NAB was supported by the ANID Grant *FONDECYT de Postdoctorado N 3230326* and by Centro de Modelamiento Matematico (CMM), Proyecto Basal FB210005.

Data availability statement

The code used in this paper is available online in a Github repository: https://github.com/nabw/navier-stokes-nitsche-vms [5].

References

[1] M.S. Alnæs, J. Blechta, J. Hake, A. Johansson, B. Kehlet, A. Logg, C. Richardson, J. Ring, M.E. Rognes and G.N. Wells, The FEniCS project version 1.5. *Arch. Numer. Softw.* **3** (2015) 2015.

[2] R. Araya, A. Caiazzo and F. Chouly, Stokes problem with slip boundary conditions using stabilized finite elements combined with Nitsche. *Comput. Methods Appl. Mech. Eng.* **427** (2024) 117037.

[3] N. Ahmed and S. Rubino, Numerical comparisons of finite element stabilized methods for a 2D vortex dynamics simulation at high Reynolds number. *Comput. Methods Appl. Mech. Eng.* **349** (2019) 191–212.

[4] I. Babuška, The finite element method with penalty. *Math. Comput.* **27** (1973) 221–228.

[5] A. Bansal and N.A. Barnafi Wittwer, Nitsche method for Navier–Stokes equations with slip boundary conditions: convergence analysis and VMS-les stabilization (source code) (2023). Available at https://github.com/nabw/navier-stokes-nitsche-vms.

[6] J.W. Barrett and C.M. Elliott, Finite element approximation of the Dirichlet problem using the boundary penalty method. *Numer. Math.* **49** (1986) 343–366.

[7] E. Bayraktar, O. Mierka and S. Turek, Benchmark computations of 3d laminar flow around a cylinder with CFX, OpenFOAM and FeatFlow. *Int. J. Comput. Sci. Eng.* **7** (2012) 253–266.

[8] Y. Bazilevs and T.J.R. Hughes, Weak imposition of Dirichlet boundary conditions in fluid mechanics. *Comput. Fluids* **36** (2007) 12–26.

[9] Y. Bazilevs, V.M. Calo, J.A. Cottrell, T.J.R. Hughes, A. Reali and G. Scovazzi, Variational multiscale residual-based turbulence modeling for large eddy simulation of incompressible flows. *Comput. Methods Appl. Mech. Eng.* **197** (2007) 173–201.

[10] S. Berg, A.W. Cense, J.P. Hofman and R.M.M. Smits, Two-phase flow in porous media with slip boundary condition. *Transp. Porous Media* **74** (2008) 275–292.

[11] S.C. Brenner and L.R. Scott, The Mathematical Theory of Finite Element Methods. Vol. 15 of *Texts in Applied Mathematics*, 3rd edition. Springer, New York (2008).

[12] E. Burman, D. Garg and J. Guzman, Implicit-explicit time discretization for Oseen's equation at high Reynolds number with application to fractional step methods. *SIAM J. Numer. Anal.* **61** (2023) 2859–2886.

[13] A. Caglar and A. Liakos, Weak imposition of boundary conditions for the Navier–Stokes equations by a penalty method. *Int. J. Numer. Methods Fluids* **61** (2009) 411–431.

[14] J. Camaño, C. García and R. Oyarzúa, Analysis of a momentum conservative mixed FEM for the stationary Navier–Stokes problem. *Numer. Methods Partial Differ. Equ.* **37** (2021) 2895–2923.

[15] F.E. Cellier and E. Kofman, Continuous System Simulation. Springer Science & Business Media (2006).

[16] F. Chouly, A review on some discrete variational techniques for the approximation of essential boundary conditions. *Vietnam J. Math.* (2024) 1–43.

[17] K.N. Christodoulou and L.E. Scriven, The fluid mechanics of slide coating. *J. Fluid Mech.* **208** (1989) 321–354.

[18] R. Codina, Stabilization of incompressibility and convection through orthogonal subscales in finite element methods. *Comput. Methods Appl. Mech. Eng.* **190** (2000) 1579–1599.

[19] R. Codina, Stabilized finite element approximation of transient incompressible flows using orthogonal subscales. *Comput. Methods Appl. Mech. Eng.* **191** (2002) 4295–4321.

[20] R. Codina, J. Principe, O. Guasch and S. Badia, Time dependent subscales in the stabilized finite element approximation of incompressible flow problems. *Comput. Methods Appl. Mech. Eng.* **196** (2007) 2413–2430.

[21] E. Colmenares, R. Oyarzúa and F. Piña. A discontinuous Galerkin method for the stationary Boussinesq system. *Comput. Methods Appl. Math.* **22** (2022) 797–820.

[22] O. Colomés, S. Badia, R. Codina and J. Principe, Assessment of variational multiscale models for the large eddy simulation of turbulent incompressible flows. *Comput. Methods Appl. Mech. Eng.* **285** (2015) 32–63.

[23] I. Dione and J.M. Urquiza, Penalty: finite element approximation of Stokes equations with slip boundary conditions. *Numer. Math.* **129** (2015) 587–610.

[24] I. Dione, C. Tibirna and J. Urquiza, Stokes equations with penalised slip boundary conditions. *Int. J. Comput. Fluid Dyn.* **27** (2013) 283–296.

[25] H.C. Elman, D.J. Silvester and A.J. Wathen, Finite Elements and Fast Iterative Solvers: With Applications in Incompressible Fluid Dynamics. *Numerical Mathematics and Scientific Computation*, 2nd edition. Oxford University Press, Oxford (2014).

[26] A. Ern and J.L. Guermond, Finite Elements I – Approximation and Interpolation. Vol. 72 of *Texts in Applied Mathematics.* Springer, Cham (2021).

[27] D. Forti and L. Dedè, Semi-implicit BDF time discretization of the Navier–Stokes equations with VMS-LES modeling in a high performance computing framework. *Comput. Fluids* **117** (2015) 168–182.

[28] G.P. Galdi and W.J. Layton, Approximation of the larger eddies in fluid motions. II. A model for space-filtered flow. *Math. Models Methods Appl. Sci.* **10** (2000) 343–350.

[29] U. Ghia, K.N. Ghia and C.T. Shin, High-re solutions for incompressible flow using the Navier–Stokes equations and a multigrid method. *J. Comput. Phys.* **48** (1982) 387–411.

[30] V. Girault and P.-A. Raviart, Finite Element Approximation of the Navier–Stokes Equations. Vol. 749 of *Lecture Notes in Mathematics.* Springer-Verlag, Berlin-New York (1979).

[31] I.G. Gjerde and L.R. Scott, Nitsche's method for Navier–Stokes equations with slip boundary conditions. *Math. Comput.* **91** (2022) 597–622.

[32] I.G. Gjerde and L.R. Scott, Kinetic-energy instability of flows with slip boundary conditions. *J. Math. Fluid Mech.* **24** (2022) 27.

[33] S. Goldstein, Modern Developments in Fluid Dynamics: An Account of Theory and Experiment Relating to Boundary Layers, Turbulent Motion and Wakes. Vol. 2. Clarendon Press (1938).

[34] H. Gopalan, S. Heinz and M.K. Stöllinger, A unified RANS-LES model: computational development, accuracy and cost. *J. Comput. Phys.* **249** (2013) 249–274.

[35] P Hansbo, Nitsche's method for interface problems in computational mechanics. *GAMM-Mitteilungen* **28** (2005) 183–206.

[36] A. Henderson, Paraview Guide: A Parallel Visualization Application. Kitware Inc. (2007).

[37] T.J.R. Hughes, L. Mazzei and K.E. Jansen, Large eddy simulation and the variational multiscale method. *Comput. Vis. Sci.* **3** (2000) 47–59.

[38] T.J.R. Hughes, A.A. Oberai and L. Mazzei, Large eddy simulation of turbulent channel flows by the variational multiscale method. *Phys. Fluids* **13** (2001) 1784–1799.

[39] V. John and A. Kindl, Variants of projection-based finite element variational multiscale methods for the simulation of turbulent flows. *Int. J. Numer. Methods Fluids* **56** (2008) 1321–1328.

[40] M. Juntunen and R. Stenberg, Nitsche's method for general boundary conditions. *Math. Comput.* **78** (2009) 1353–1374.

[41] T. Kashiwabara, I. Oikawa and G. Zhou, Penalty method with P1/P1 finite element approximation for the Stokes equations under the slip boundary condition. *Numer. Math.* **134** (2016) 705–740.

[42] T. Kashiwabara, I. Oikawa and G. Zhou, Penalty method with Crouzeix–Raviart approximation for the Stokes equations under slip boundary condition. *ESAIM Math. Model. Numer. Anal.* **53** (2019) 869–891.

[43] B. Koobus and C. Farhat, A variational multiscale method for the large eddy simulation of compressible turbulent flows on unstructured meshes application to vortex shedding. *Comput. Methods Appl. Mech. Eng.* **193** (2004) 1367–1383.

[44] W. Layton, Weak imposition of "no-slip" conditions in finite element methods. *Comput. Math. Appl.* **38** (1999) 129–142.

[45] H. Minaki and S. Li, Multiscale modeling and simulation of dynamic wetting. *Comput. Methods Appl. Mech. Eng.* **273** (2014) 273–302.

[46] A. Montlaur, S. Fernandez-Mendez, J. Peraire and A. Huerta, Discontinuous Galerkin methods for the Navier–Stokes equations using solenoidal approximations. *Int. J. Numer. Methods Fluids* **64** (2010) 549–564.

[47] R.C. Moura, G. Mengaldo, J. Peiró and S.J. Sherwin, On the eddy-resolving capability of high-order discontinuous Galerkin approaches to implicit LES/under-resolved DNS of Euler turbulence. *J. Comput. Phys.* **330** (2017) 615–623.

[48] J. Nitsche, Über ein Variationsprinzip zur Lösung von Dirichlet-Problemen bei Verwendung von Teilräumen, die keinen Randbedingungen unterworfen sind. *Abh. Math. Sem. Univ. Hamburg* **36** (1971) 9–15.

[49] M.R. Nived, S.S.C. Athkuri and V. Eswaran, On the application of higher-order backward difference (BDF) methods for computing turbulent flows. *Comput. Math. Appl.* **117** (2022) 299–311.

[50] X. Nogueira, L. Cueto-Felgueroso, I. Colominas and H. Gómez, Implicit large eddy simulation of non-wall-bounded turbulent flows based on the multiscale properties of a high-order finite volume method. *Comput. Methods Appl. Mech. Eng.* **199** (2010) 615–624.

[51] S. Perdoncin, Numerical validation of a variational multiscale-LES turbulence model for blood flows. *POLITesi* (2020).

[52] A. Quarteroni, R. Sacco and F. Saleri, Matematica Numerica. Springer-Verlag Italia, Milan (1998).

[53] W. Rodi, DNS and LES of some engineering flows. *Fluid Dyn. Res.* **38** (2006) 145–173.

[54] L. Scott, Introduction to Automated Modeling with FEniCS. Computational Modeling Initiative LLC (2018).

[55] Z.C. Shi, On the convergence rate of the boundary penalty method. *Int. J. Numer. Methods Eng.* **20** (1984) 2027–2032.

[56] Y. Sone, Kinetic Theory and Fluid Dynamics. Springer (2002).

[57] R. Stenberg, On some techniques for approximating boundary conditions in the finite element method. *J. Comput. Appl. Math.* **63** (1995) 139–148.

[58] A. Tagliabue, L. Dedè and A. Quarteroni, Isogeometric analysis and error estimates for high order partial differential equations in fluid dynamics. *Comput. Fluids* **102** (2014) 277–303.

[59] V. Thomée, Galerkin Finite Element Methods for Parabolic Problems. Vol. 1054 of *Lecture Notes in Mathematics*. Springer-Verlag, Berlin (1984).

[60] J.M. Urquiza, A. Garon and M.I. Farinas, Weak imposition of the slip boundary condition on curved boundaries for Stokes flow. *J. Comput. Phys.* **256** (2014) 748–767.

[61] R. Verfürth, Finite element approximation on incompressible Navier–Stokes equations with slip boundary condition. *Numer. Math.* **50** (1986) 697–721.

[62] R. Verfürth, Finite element approximation of incompressible Navier-Stokes equations with slip boundary condition. II. *Numer. Math.* **59** (1991) 615–636.

[63] J. Volker, Higher order finite element methods and multigrid solvers in a benchmark problem for the 3D Navier–Stokes equations. *Int. J. Numer. Methods Fluids* **40** (2002) 775–798.

[64] J. Volker, On the efficiency of linearization schemes and coupled multigrid methods in the simulation of a 3D flow around a cylinder. *Int. J. Numer. Methods Fluids* **50** (2006) 845–862.

[65] T. Warburton and J.S. Hesthaven, On the constants in hp finite element trace inverse inequalities. *Comput. Methods Appl. Mech. Eng.* **192** (2003) 2765–2773.

[66] M. Winter, B. Schott, A. Massing and W.A. Wall, A Nitsche cut finite element method for the Oseen problem with general Navier boundary conditions. *Comput. Methods Appl. Mech. Eng.* **330** (2018) 220–252.

[67] G. Zhou, T. Kashiwabara and I. Oikawa, Penalty method for the stationary Navier–Stokes problems under the slip boundary condition. *J. Sci. Comput.* **68** (2016) 339–374.

[68] G. Zhou, T. Kashiwabara and I. Oikawa, A penalty method for the time-dependent Stokes problem with the slip boundary condition and its finite element approximation. *Appl. Math.* **62** (2017) 377–403.

[69] G. Zhou, I. Oikawa and T. Kashiwabara, The Crouzeix–Raviart element for the Stokes equations with the slip boundary condition on a curved boundary. *J. Comput. Appl. Math.* **383** (2021) 113123.